ACS APPLIED MATERIALS & INTERFACES

www.acsami.org Research Article

Soft Magnetic Microrobot Doped with Porous Silica for Stability-Enhanced Multimodal Locomotion in a Nonideal Environment

Shangsong Li, Dong Liu, Yuping Hu, Zhijie Su, Xinai Zhang, Ruirui Guo, Dan Li, and Yuan Lu*

Cite This: https://doi.org/10.1021/acsami.1c25102 Read Online

ACCESS | Metrics & More | Article Recommendations | Supporting Information

ABSTRACT: As an emerging field of robotics, magnetic-field-controlled soft microrobot has broad application prospects for its flexibility, locomotion diversity, and remote controllability. Magnetic soft microrobots can perform multimodal locomotion under the control of a magnetic field, which may have potential applications in precision medicine. However, previous research studies mainly focus on new locomotion in a relatively ideal environment, lacking exploration on the ability of magnetic microrobot locomotion to resist external disturbances and proceed in a nonideal environment. Here, a porous silica-doped soft magnetic microrobot is constructed for enhanced stability of multimodal locomotion in the nonideal biological environment. Porous silica spheres are doped into a NdFeB−silicone elastomer base, improving adhesion properties and refining the comprehensive mechanical properties of the microrobot. Multimodal locomotions are achieved, and the influence of porous silica doping on the stability of each locomotion in a nonideal environment is explored in depth. Motions in nonideal circumstances such as climbing, loading, current rushing, wind blowing, and obstacle hindering are conducted successfully with porous silica doping. Such a stability-enhanced multimodal locomotion system can be used in biocatalysis and thrombus removal, and its prospect for precision medicine is highlighted by in vivo demonstration of multimodal locomotion with nonideal disturbance.

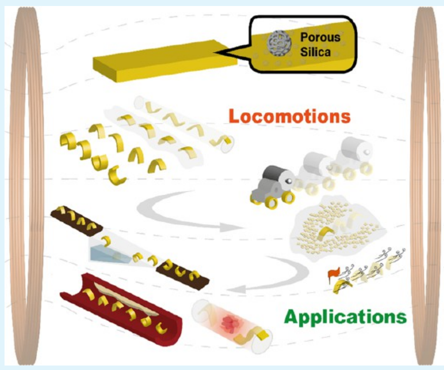

KEYWORDS: *soft magnetic microrobot, multimodal locomotion, porous silica, doping, nonideal biological environment*

■ INTRODUCTION

Due to outstanding flexibility, locomotion diversity, and remote controllability, a magnetic soft microrobot has broad application prospects. Under the control of the external magnetic field, a micromagnetic soft robot can perform multimodal locomotion, including basic movement patterns such as walking, jumping, rolling, and swimming. This brings theoretical possibility to the application of a magnetic soft microrobot in various areas. Especially, microrobots have potential applications in precision medicine,[1] including minimally invasive surgery,[2] drug delivery,[3] and cancer treatment,[4] contributing to human health. The advantages of soft magnetic microrobots are obvious. First, microrobots are usually limited to millimeters or even micrometers. This miniaturization makes it easy to enter certain parts of a complex structure, especially narrow ones such as small intestine and microchemical tubes, reducing the complexity of the entry process.[5] Due to the small size, its movement will have high flexibility and experience little hindrance, not causing damage to surroundings. Second, since the control of microrobot movement is realized by the magnetic field, which can easily penetrate the blockings without causing additional changes, the safety and effectiveness of the method are ensured.[6] By changing the magnitude and direction of the magnetic field, various locomotions of the robot can be achieved, and suitable locomotion can be used in different environments to accomplish the whole task.[7]

For the research of a magnetic soft robot, a lot of attention has been paid on creating new locomotions, such as jellyfish-like swimming,[8] helical propulsion,[9] flapping,[10] and rotating.[11] These studies provided innovation in the basic level of locomotion and broadened the application possibility of magnetic microrobots. However, a common problem is that although many locomotions could be achieved, for excellent display effect, the locomotions involved in previous studies were basically completed in a relatively ideal environment, such as walking on a flat surface, rolling on a normal substrate, and swimming in still water. In fact, the stability of locomotion in a nonideal environment is greatly important because in a real internal environment, the moving magnetically controlled flexible robot will be affected by various disturbances, including but not limited to muscle peristalsis, air flow impact, liquid flow impact, obstacle barrier, sudden change of physical

Received: December 28, 2021
Accepted: February 10, 2022

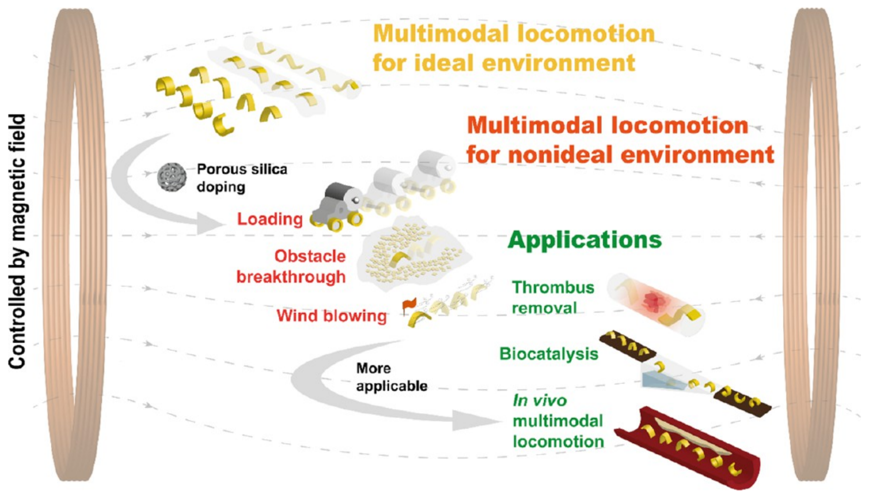

Figure 1. Overall illustration of the p-Si-doped soft magnetic microrobot for enhanced stability of multimodal locomotion in a nonideal biological environment. As is mentioned in the figure, the inner core of the research design is, with the method of p-Si doping, upgrading the previous microrobotic locomotion for only ideal environment to locomotion in a nonideal environment including but not limited to cargo loading, obstacle crossing, and wind blowing, which can be more applicable to practical scenarios such as thrombus removal, biocatalysis, and in vivo targeted therapy. Magnetic field control is necessary from the beginning to the end.

properties of the base, steep slope, and sharp turn. A robot walking normally in an ideal environment may slip or even fall under the impact of water flow. Regarding the ability of magnetic microrobot locomotion to resist external disturbances and proceed in a nonideal environment, unfortunately, there is a lack of relevant studies, which is unfavorable to the practical application of micromagnetron robots in precision medicine.

In order to solve the aforementioned problem of locomotion stability in a nonideal environment, two options could be considered. The first option is to adjust the external magnetic field according to the change in the environment, keeping the robot at a relatively stable situation. However, this idea is difficult to realize in practice because the microrobot needs to face the complex and changeable actual environment in various tasks. With a deep reinforcement learning method, it is still difficult to give an appropriate and timely response to various environmental changes in a microscale biological environment.[12] The second option is to control the performance of the robot body material to enhance its adhesion to substrate and improve its mechanical properties. In this way, the motion stability of the microrobot can be improved greatly. In fact, material modification by doping is a common method to improve material properties and prepare new materials.[13] For the improvement of adhesion properties, nonmetallic inclusions with high porosity and rough microsurface can be introduced, such as porous silica (p-Si) rods[14] or spheres[15] (Text S1). The regulation of the matrix polymer itself may also improve adhesion.[16] However, the modification of soft materials often pointed to applications such as flexible electronics[17] and percutaneous drug delivery.[14] In previous studies, unfortunately, there is no research directly combining material doping modification with multimodal locomotion of soft magnetic microrobots (Figure 1).

Here, a soft magnetic microrobot with p-Si doping was first reported for stability-enhanced multimodal locomotion in a nonideal environment. p-Si spheres were doped into the NdFeB−silicone rubber base, improving adhesion properties and refining comprehensive mechanical properties of the magnetic soft microrobot. Basic multimodal locomotions including rolling, walking, jumping, and crawling were achieved, and the influence of p-Si doping on the stability of each locomotion in a nonideal environment was explored in depth. With the stability data of each locomotion, basic locomotions could be assembled into more complex locomotions (drifting, stirring, trolley, and boat) via rational design, enlarging the locomotion library while achieving more complex tasks. Different from previous action demonstrations in an ideal environment, among the locomotion library of this research, motions could be conducted in nonideal circumstances such as climbing, loading, current rushing, wind blowing, and obstacle hindering. Such a stability-enhanced multimodal locomotion system could be used in biocatalysis and thrombus removal, and its prospect for precision medicine was highlighted by in vivo demonstration of multimodal locomotion with nonideal disturbance.

RESULTS AND DISCUSSION

Material Synthesis and Characterization. The material of magnetic microrobots, including both base material and doping material, was synthesized and characterized. For the base material of the robot body, neodymium iron boron (NdFeB) magnetic microparticles were mixed with the Ecoflex 00−10 polymer matrix A and B (a kind of silicone rubber) according to the mass ratio of 1:1.[1] NdFeB microparticles provided the ability for magnetic control, while the Ecoflex 00−10 polymer matrix made up the viscoelastic and biocompatible body (Figure 2a). When the raw materials were initially mixed, the mixture was liquid. After standing in the air for 3−5 h, silicone was cross-linked, forming a silica network. Eventually, the mixture was solidified into silicone rubber and made into pieces of microrobots (Figure 2b). p-Si microparticles were synthesized via a traditional method[18] and doped into the robot body with a concentration gradient of 0, 0.3, 0.6, 0.9, and 1.2 wt %. Because of the porous and loose surface (Figure 2c,d), p-Si may effectively hinder the movement of molecular chains in the viscoelastic matrix so as to improve the viscosity and refine mechanical properties of the robot. From the macroscale, NdFeB was uniformly mixed in the silica matrix. However, from the microscale, obvious

https://doi.org/10.1021/acsami.1c25102
ACS Appl. Mater. Interfaces XXXX, XXX, XXX−XXX

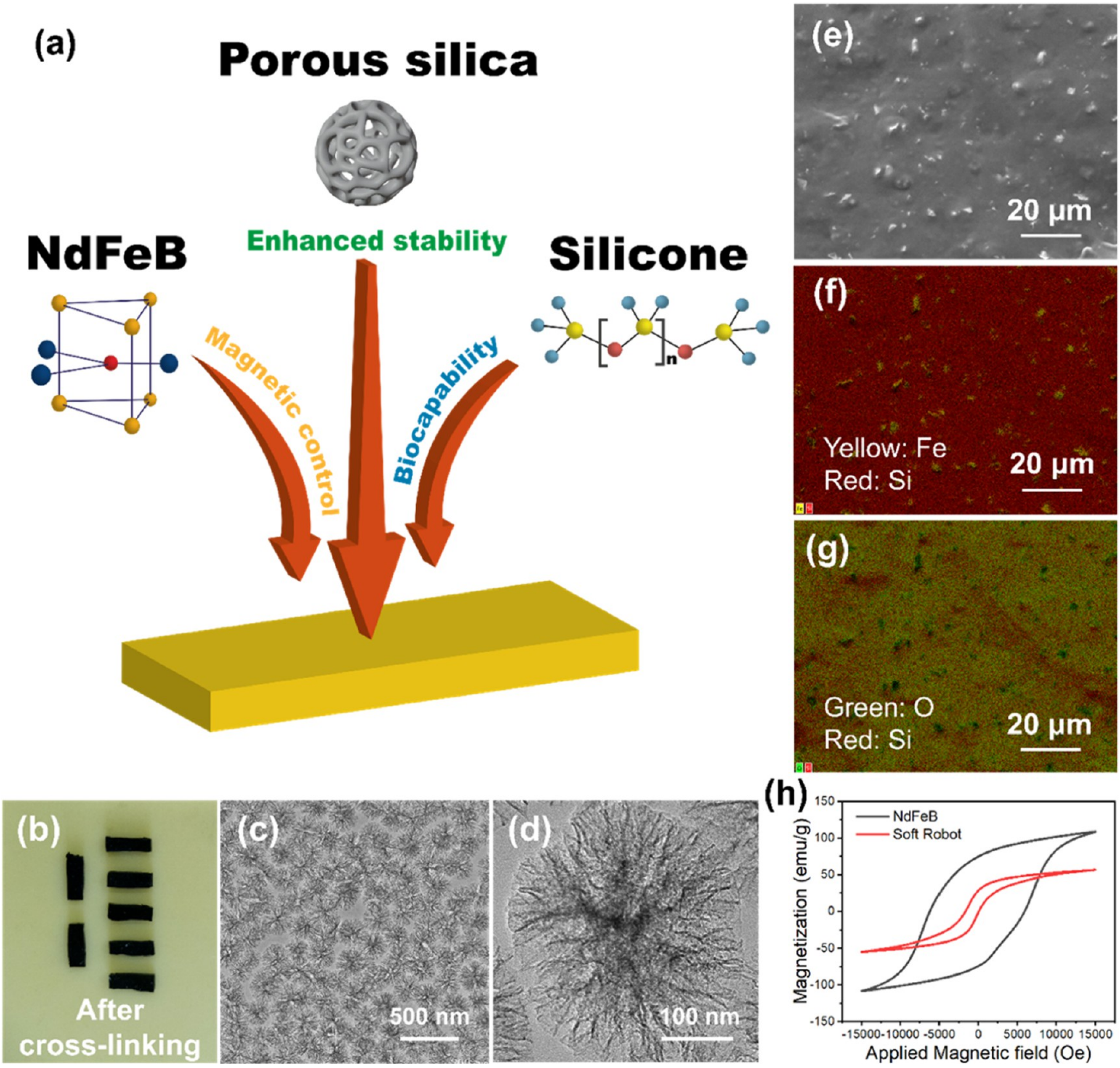

Figure 2. Material synthesis and characterization. (a) Illustration of materials composing the microrobot. (b) Solid mixture cut into pieces of microrobots after cross-linking. (c) Transmission electron microscopy (TEM) image of p-Si nanoparticles, low-magnification. (d) TEM image of the p-Si nanoparticle, high-magnification. (e) SEM image for the quenched section of the magnetic soft robot. (f) Energy-dispersive spectrometry (EDS) image of the magnetic soft robot, showing the distribution of the Fe (yellow) and Si (red) elements. (g) EDS image of the magnetic soft robot, showing the distribution of the O (green) and Si (red) elements. (h) Magnetic hysteresis loops of NdFeB and magnetic soft robots.

segregation was observed via a scanning electron microscopy (SEM) picture of the quenched section (Figure 2e). Element mapping of Si, Fe, and O elements further confirmed the granular distribution of NdFeB microparticles (Figure 2f−g). Magnetic response measurements using a vibrating sample magnetometer (Figure 2h) showed the classical hysteresis loop of hard magnetic materials, as well as gave the magnetization saturation value of 109.4 emu/g for NdFeB and 56.9 emu/g for the magnetic soft robot, indicating strong response to the magnetic field.

Mechanical Properties. Mechanical properties of silica elastomers were investigated via tensile test (Figure 3b, Video S1) and tensile-adhesion test (Figure 3a,c). Four groups of tensile properties, elongation, toughness, tensile strength, and elastic modulus, were calculated according to the stress−strain curves (Figure 3d). When the concentration of doped p-Si increased from zero, the elongation (Figure 3e) and toughness (Figure 3f) of the silica elastomer showed an obvious upward trend, maximized by the p-Si incorporation of 0.9 wt % and then declined for 1.2 wt %. The results could be explained intuitively that after embedded with different concentrations of p-Si (from 0 to 1.2 wt %), silica elastomers became softer and easier to extend and were harder to break when stretching slowly. To a certain extent, it avoided the soft robot to be broken by some small but continuous tension. Meanwhile, the tensile strength (Figure 3g) and elastic modulus (Figure 3h)

https://doi.org/10.1021/acsami.1c25102
ACS Appl. Mater. Interfaces XXXX, XXX, XXX−XXX

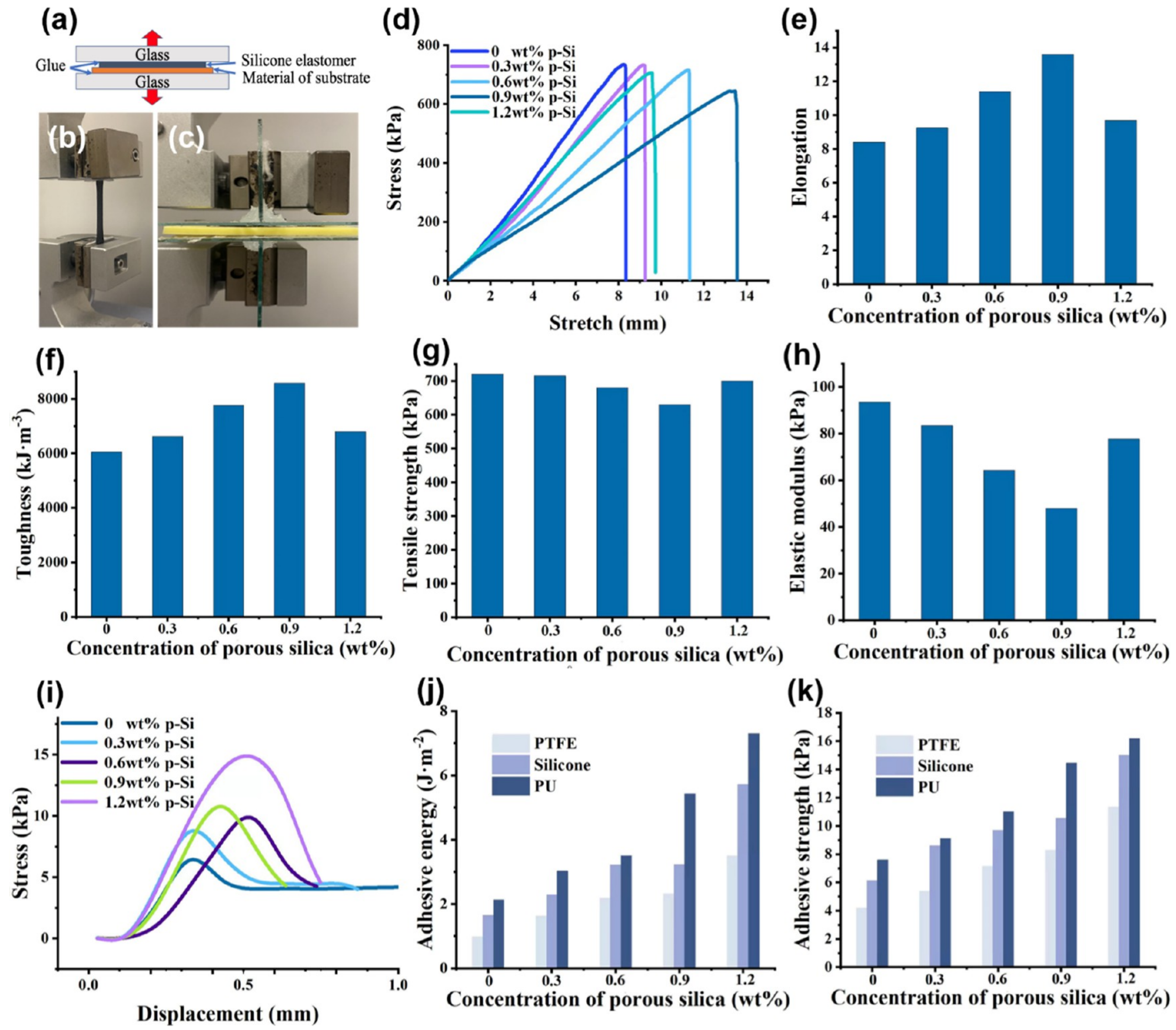

Figure 3. Characterization of mechanical properties of the microrobot material. (a) Illustration of the tensile-adhesion test. (b) Capture of the tensile test. (c) Capture of the tensile-adhesion test. (d) Stress−strain curve for the tensile test. (e) Bar graph showing the relationship between elongation and p-Si concentration. (f) Bar graph showing the relationship between toughness and p-Si concentration. (g) Bar graph showing the relationship between tensile strength and p-Si concentration. (h) Bar graph showing the relationship between elastic modulus and p-Si concentration. (i) Stress−strain curve for the tensile-adhesion test on the PU substrate. (j) Bbar graph showing the adhesive energy for the microrobot material with different concentrations of p-Si doping on three different substrates (PTFE, silicone, and PU). (k) Bar graph showing the adhesive strength for microrobot material with different concentrations of p-Si doping on three different substrates (PTFE, silicone, and PU).

decreased with the increase in p-Si concentration. The decline in the elastic modulus was relatively significant. Decreasing the elastic modulus indicated that the soft robot was easier to produce elastic deformation under stress. Summarily, p-Si doping could refine mechanical properties by softening the robot body with the best soften effect at 0.9 wt %, so it was feasible to dope p-Si in the silicon elastomer.

For the enhancement of locomotion stability, more adhesion to the substrate was required. p-Si doping was a method to improve adhesion via rational design. The enhanced adhesiveness of silicone elastomers through incorporation of p-Si was investigated by a tensile-adhesion test.[15] Silicone elastomers embedded with different concentrations of p-Si (from 0 to 1.2 wt %) were freshly prepared. Thereafter, the silicone elastomer was attached to different substrates, and the adhesiveness was measured through the stress−strain curve (Figures 3i, S4). Three materials of substrate were selected in the test: biomimetic silicone gel close to skin texture (hereinafter referred to as silica gel), medical polyurethane (hereinafter referred to as PU), and medical polytetrafluoroethylene (hereinafter referred to as PTFE). Such a substrate selection was meaningful for exploring the application prospects of microrobots in biomedicine. Subsequently, the differences of microrobot locomotions with gradient concentrations on these substrates were also discussed to explore whether the results corresponded to the measurements of mechanical properties of these three substrates. Biomimetic silica gel could work as a good simulation for skin texture.[19] PU has good wear resistance, toughness, excellent corrosion resistance and chemical resistance, soft tissue compatibility,

https://doi.org/10.1021/acsami.1c25102
ACS Appl. Mater. Interfaces XXXX, XXX, XXX−XXX

and blood compatibility. It could be used as medical hose, bone repair material, supplementary material for vascular surgical suture, and the main constituent material of the artificial heart and artificial kidney.[20] PTFE is the main material of artificial blood vessels.[21] Therefore, PU and PTFE could well-simulate the human internal environment for microrobot locomotion. With silicone elastomers attached to three different substrates, the adhesive strength increased on increasing the concentration of incorporated p-Si (Figure 3k), and the adhesive energy increased more significantly (Figure 3j). The maximum adhesive energy on the PU substrate, 7.3 J/m^2, appeared at 1.2 wt % p-Si concentration, which was approximately 2.5 times higher than that of 0 wt %. The tensile-adhesion test indicated that p-Si doping evidently increased adhesiveness of the silica elastomer.

Fabrication of Flexible Micromagnetron Robots for Multimodal Locomotion. To achieve various locomotions, a harmonic magnetization profile $\boldsymbol{m}$ was embedded in the robot body. The robot was wrapped with a cylindrical wood rod, whose circumference was 3.7 mm. Meanwhile, a proper phase shift β was significantly important.[1] The bottom was defined as 0°, and via calculation, the default phase shift β was set to 45° in the following research unless specially clarified. The properly wrapped robot was placed into a pulse magnetizer for magnetization with a strong, directional, uniform magnetic field $\boldsymbol{B}$ of 2.5 T (Figures 4a, S5).

The dispersed NdFeB microparticles were magnetized into the same direction. Hence, after unwrapping, a robot body with the harmonic magnetization profile $\boldsymbol{m}$ would be achieved, and the dimension of the microrobot was 0.2 × 1.5 × 3.7 mm (Figure 4b). Owing to these features, different locomotions could be achieved by applying an alternating magnetic field $\boldsymbol{B} = [B_x, B_y, B_z]^{\mathrm{T}}$ in an electromagnetic setup, which contained three pairs of orthogonal Helmholtz coils (Figure S6). By adjusting the voltage applied on each coil, the magnetic field intensity could be controlled properly to actuate the magnetic microrobot.

The moving state of magnetic microrobots was greatly complicated, and it was nearly impossible to give a reasonable kinematic analysis of magnetic microrobots under any external conditions, including but not limited to magnetization profile, magnetic field, and friction. However, the problem could be solved from a different perspective. If several basic locomotions were explored in advance, then complex multitasking locomotion could be achieved by rationally combining the basic locomotions together. Previous studies have proved that microrobot locomotions such as rolling, jumping, walking, and crawling are basic locomotions.[1] Due to mathematical simplification of locomotion design, they could be verified by both theoretical calculations and experiments. Moreover, these locomotions could be used in most practical scenarios. For this research design, using p-Si to stabilize the performance of microrobots, if the stability of microrobot performance needed evaluation, the reasonable solution was to check stability for each basic locomotion. Supposing that every basic locomotion became more stable after p-Si doping, then it would be concluded that p-Si could indeed stabilize the performance of microrobots. Besides rolling, jumping, walking, and crawling, which have been given in previous studies, new locomotions of drifting and stirring that made microrobots suitable for moving in liquid were also designed, and stability for the two new locomotions after p-Si doping was explored.

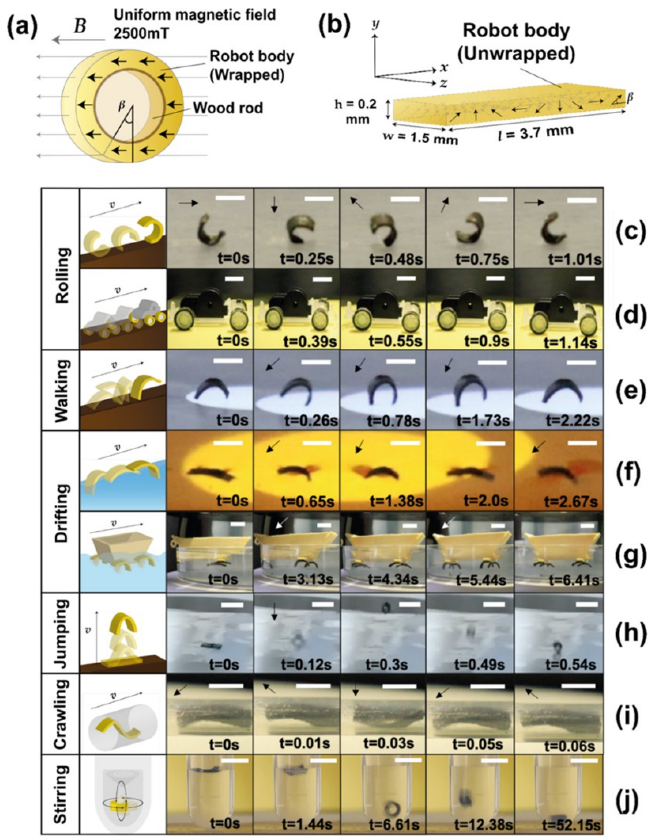

Figure 4. Schematic of magnetization and different locomotions. (a) Robot is wrapped by a wood rod when magnetizing. (b) Robot is unwrapped and showing the magnetization profile $\boldsymbol{m}$. (c) Rolling locomotion, with a rotating magnetic field $\boldsymbol{B}_{xz}$. Scale bar, 2 mm. (d) Trolley assembled by four rolling robots. Scale bar, 1 cm. (e) Walking locomotion, induced by a three-phase magnetic field. Scale bar, 2 mm. (f) Drifting locomotion, induced by a three-phase magnetic field. Scale bar, 2 mm. (g) Boat assembled by four drifting robots. Scale bar, 2 mm. (h) Jumping locomotion, induced by a large deformation. Scale bar, 5 mm. (i) Crawling locomotion with a rotating magnetic field. Scale bar, 2 mm. (j) Stirring locomotion, with three orthogonal axes of the rotating magnetic field. Scale bar, 8 mm.

An overall description of multimodal locomotion was shown (Figure 4c−j) which illustrated time-dependent captures of each locomotion. In addition, the general theory and mathematical analysis are appended in the Supporting Information (Text S2). In rolling locomotion (Figure 4c, Video S2), a rotating magnetic field $\boldsymbol{B}_{xz}$ (f = 3 Hz and B = 8 mT) was applied. Compared to other locomotions, rolling locomotion was an efficient and stable way to move (Figure 4c). Moreover, microrobots were capable to overcome rough terrains via rolling locomotion, especially moving on bionic tissue which would be further discussed later. For more complex locomotion, four robots were rationally designed as the four wheels of a magnetic controlled trolley (Figure 4d, Video S3). The trolley could move smoothly on most substrates and even deliver cargoes.

Walking locomotion was inspired by inchworms (Figure 4e and Video S4), by applying a periodic magnetic field $\boldsymbol{B}_{xy}$, which presented an increase−invariant−decrease trend in magnitude and invariant−decrease−invariant in the angle of the direction α ($B_{\max}$ = 10 mT, $B_{\min}$ = 0 mT, $\alpha_{\max}$ = 150°, and $\alpha_{\min}$ = 120°). Moreover, mesoporous silica doping played a positive role in walking locomotion by reinforcing the friction.

https://doi.org/10.1021/acsami.1c25102
ACS Appl. Mater. Interfaces XXXX, XXX, XXX−XXX

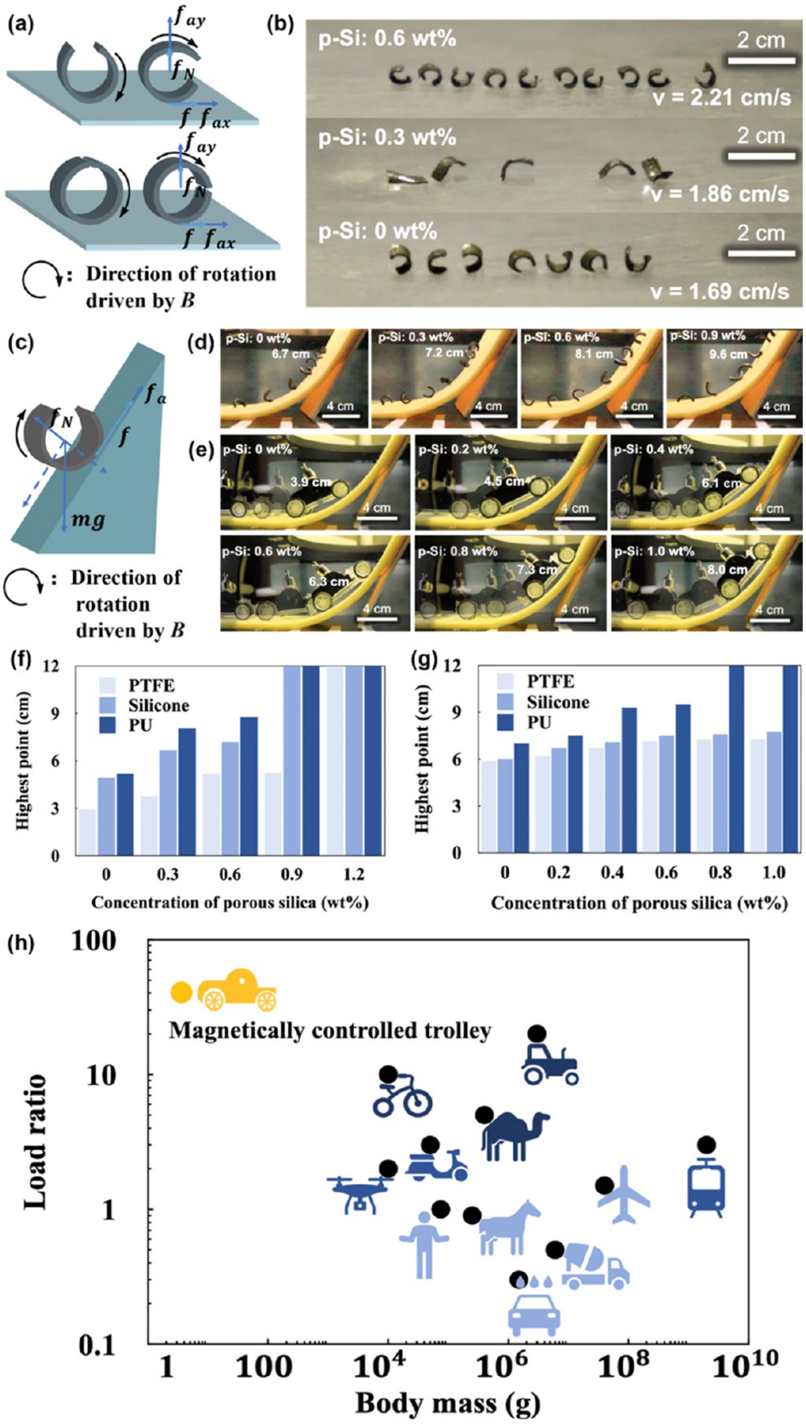

Figure 5. Influence of the p-Si doping on rolling locomotion. (a) Mechanical analysis of rolling locomotion on the flat surface. (b) Comparison of the rolling effect on the flat surface for different concentrations of p-Si doping. (c) Mechanical analysis of rolling locomotion on a slope. (d) Comparison of rolling effect on a slope for different concentrations of p-Si doping. (e) Comparison of rolling effect of a magnetically controlled trolley on a slope for different concentrations of p-Si doping. (f) Bar graph showing the highest reaching point of rolling locomotion for different doping concentrations and different substrate materials. (g) Bar graph showing the highest reaching point of a magnetically controlled trolley for different doping concentrations and different substrate materials. (h) Illustration of the comparison for load ratio between a magnetically controlled trolley and common transportations.

For the movement in an actual biological environment, microrobots should be able to move not only move on land but also in liquid. The microrobot in this research was made of a hydrophobic material; consequently, it could float on liquid, especially liquid with high surface tension. By applying the same magnetic field as walking locomotion did on a floating robot, drifting locomotion was achieved (Figure 4f, Video S5). Via this locomotion, the microrobot could move quickly, which was coincidentally familiar to Gerridae and there were a few applications in vivo such as drifting in blood vessels, GI tract, and so forth. Similar to the trolley mentioned above, four robots were rationally designed to assemble into a tiny magnetic-controlled boat (Figure 4g and Video S5), which might provide an excellent outlet for drug delivery in vivo.

Jumping locomotion could be classified into two ways (Figure 4h, Video S6), vertical jumping and horizontal jumping. For vertical jumping, the robot was magnetized with phase shift $\beta = -90°$, and a magnetic field controlled by DC power with $\alpha = 270°$ (perpendicular to the ground) should be applied. For horizontal jumping, the phase shift β was 0°, and the direction of the applied magnetic field was the same as that of vertical jumping. The magnitude of the magnetic field in both kinds of jumping was large in order to actuate enough deformation at the initial state. Via the combination of vertical and horizontal jumping, microrobots could effectively jump over obstacles, achieving more places not to be reached by rolling or walking.

Crawling locomotion could be achieved by applying an alternative magnetic field $\boldsymbol{B}_{xz}$ with $f = 15$ Hz and $B = 10$ mT (Figure 4i and Video S7). By placing the robot in a glass tunnel with a radius $r = 0.6$ mm, the robot would crawl like a travelling wave with confined phase transfer actuated by the rotating magnetic field. Crawling locomotion might contribute to invasive surgery for its ability to remove thrombus in blood vessels.

Stirring locomotion, with the fundamental of rolling locomotion, was controlled by magnetic field rotating periodically in three consecutive planes (*xy*, *xz*, and *yz* planes). As a result, it enabled the microrobot to stir adequately in order to increase the reaction rate in a small reactor (Figure 4j and Video S8). Stirring locomotion is promising for intelligent microchemical engineering systems by replacing traditional magnetic stirrers and might also be used for targeted therapy via oriented biocatalysis.

Although there were various locomotions to achieve, p-Si doping could always enhance locomotion stability, making microrobots more adaptive in a nonideal environment. For rolling and walking locomotions, p-Si doping could directly increase the friction between the microrobot body and substrate, thus making the locomotion more stable. For other locomotions, the effect of p-Si doping-induced stability was mainly because p-Si could soften the microrobot body and increase flexibility. The enhanced flexibility reduced the effect of disturbance from the surroundings, making microrobots smoother to move forward.

Rolling Locomotion and Magnetic-Controlled Trolley. The magnetization orientation of the microrobot was a trigonometric function expanded by a circle; then, the microrobot might return to the arc shape and go forward by applying an appropriate sine−cosine varying magnetic field. This led to the microrobot being most suitable for rolling dynamics in essence, and other locomotions were derived from rolling locomotion by tumbling of certain parts in a more complex magnetic field. By means of rolling, the microrobots could achieve maximum moving efficiency due to little friction losses and easy acceleration.[22] Thus, rolling became the major locomotion for microrobots in this study.

The soft robot could roll directionally in a C-shape configuration (Figure 4c, Video S2), enabled by a rotating magnetic field, which was the rolling locomotion. Similarly, the robot was connected end to end to form a circular shape which could further become part of a magnetic-controlled trolley. Doped p-Si could effectively improve rolling locomotion under the circumstances of relatively small friction or large resistance, which was possibly attributed to enhanced adhesion. According to basic mechanical analysis (Figure 5a), while rolling individually or as a magnetic-controlled trolley, microrobot locomotion was mainly affected by three forces: magnetic force, frictional force (represented as $\boldsymbol{f}$ in Figure 5a), and adhesive force (represented as $\boldsymbol{f}_{ax}$ and $\boldsymbol{f}_{ay}$ in Figure 5a). Magnetic force enabled the robot to rotate in situ, and frictional force made it possible for the robot to move forward (Text S3). The essence of adhesive force was intermolecular attraction.[23] During the macroscopic rolling locomotion, adhesive force could be decomposed into two orthogonal component forces. One was along the direction of motion, and the other was perpendicular to the direction of motion, pointing to the contact surface. The former component had the same effect as friction, that is, the driving force to let the robot move forward. Due to the difference in order of magnitude, the latter component could be reasonably ignored in analysis. According to experimental results (Figure 3), doped p-Si could effectively improve the adhesion of microrobots to specific materials (PTFE, PU, and silica). This helped with rolling locomotion under a small frictional force or large resistance. It was natural to consider these circumstances, as there were many surfaces of the human body with a low friction coefficient, such as sweat-soaked skins, mucus-covered organ walls, and lipid-rich organs. Additionally, the rolling locomotion went well under a wide range of friction and resistance, which further broadened the applicability of microrobots in a complex human environment. In this study, three groups of experiments were conducted to verify the abovementioned theory.

First, oleic acid was added to the surface of a weighing paper to construct a substrate with relatively little friction for rolling locomotion. Robots rolled in different speeds with different concentrations of doped p-Si (Figure 5b). Those with higher concentrations of p-Si had a larger adhesive force, which offset the decrease in frictional force due to the oiled paper substrate and effectively avoided slipping, thus increasing the rolling speed.

Second, resistance was set up with a slope. A simple slope was built to change the effect of gravity on robots' rolling locomotion, and the slope structure could be an approximation for some steep motion paths of microrobots in the human body. According to mechanical analysis of the robot rolling forward on slope (Figure 5c), gravity (represented as $\boldsymbol{mg}$ in Figure 5c) could be decomposed into two orthogonal components. The gravity component in the vertical motion direction for the slope surface was smaller than the whole gravity $\boldsymbol{mg}$ on the flat surface, which reduced the friction. More importantly, the component parallel to the motion direction greatly resisted the rolling locomotion. Considering the abovementioned factors, adhesive force became even more prominent. In the experiment, three different materials were used as slope substrates. Material type of substrate and concentration of doped p-Si were treated as two variables, and the distance between the highest point that microrobots rolled to and the upper surface of the horizontal part for the substrate was measured (Figure 5f). For the angle of slope, 30, 45, and 60° were chosen as experimental groups. Results of different slope angles had a similar trend for comparison of different doping concentration and substrates, but comparison effect at 60° turned to be the best and was shown here. Results for 30 and 45° are listed in the Supporting Information (Figures S7, S9). It was found that the locomotion could well-correspond to the material synthesis and mechanical analysis: the greater the

https://doi.org/10.1021/acsami.1c25102
ACS Appl. Mater. Interfaces XXXX, XXX, XXX−XXX

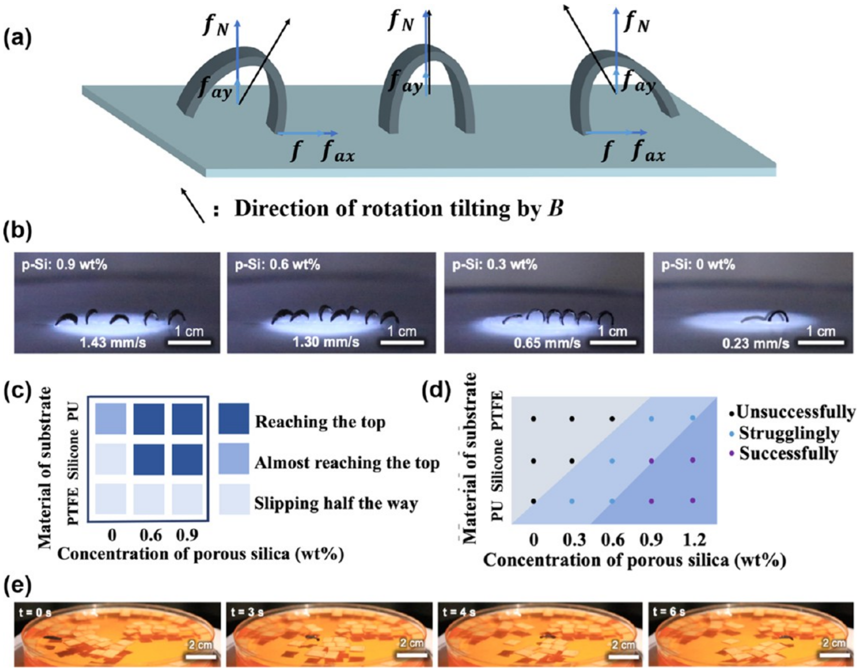

Figure 6. Influence of p-Si doping on walking locomotion. (a) Mechanical analysis of walking locomotion on the flat surface. (b) Comparison of walking effect on the flat surface for different concentrations of p-Si doping. (c) Color block diagram showing the situation of walking locomotion for different doping concentrations and different substrate materials. (d) Lattice diagram showing the stability of walking locomotion for different doping concentrations and different substrate materials when encountering wind blowing. (e) Captures showing the process of breaking through obstacles ahead via drifting locomotion.

adhesion between the robot body and substrate material, the better the rolling locomotion state (faster speed and more stable posture). Moreover, microrobot rolling locomotion could overcome steep slope better (higher position and steeper angle) via p-Si doping.

Third, resistance was set up with a slope for magnetic-controlled trolley. If the robot was connected end to end to form a circular shape, then it could replace tires, assembling into a magnetic-controlled trolley. Compared with a single robot, a magnetic-controlled trolley could realize more powerful functions. Under magnetic control, it could transport and unload cargoes (Video S3). Moreover, its load ratio could exceed 40, far larger than that of common transportations (Figure 5h), which showed the great strength of magnetic control. The slope experiments for magnetic-controlled trolley also took material type of substrate and doping concentration of porous silicon as two variables, and vertical climbing height for a slope angle of 60° was measured (Figures 5e, S8, S10). It was found that the greater the adhesion between the robot body and substrate material, the better the magnetic-controlled trolley could move forward (Figure 5g).

From the three abovementioned experiments, it could be concluded that for rolling locomotion and its derivative application (magnetic-controlled trolley), adhesion had a positive influence, which was especially significant when encountering deficient frictional force or obvious resistance. Also, p-Si doping helped with it by improving the adhesion of the robot body to substrate material.

Particularly, as the essence of adhesion was attraction, when the adhesion force was too large, it was negative to mutual displacement between the robot and the substrate. Moreover, with p-Si doping reducing the rigidity of the microrobot, the contact surface between the microrobot and substrate enlarged, which further increased the adhesion force, thus hindering the rolling locomotion. This was verified by the experiment in which dry weighing paper instead of oiled paper was taken as the substrate. Dry weighing paper was rough enough and had appreciable adhesion with soft robots. Driven by magnetic force, robots with higher concentrations of doped p-Si rolled more slowly and even hard to move forward on dry weighing paper (Video S3), which gave an opposite trend compared to the results for oiled paper.

Walking Locomotion, Drifting Locomotion, and Magnetically Controlled Boat. Rolling locomotion was important for it was the most effective way of marching. However, considering the small dimension of the micro-environment, the speed of rolling was relatively fast. Therefore, apart from rolling, a slower way of going forward was also needed to enhance the overall control accuracy.[24] In fact, driven by a periodical magnetic field, microrobots could walk rightward, as shown in Figure 6b, which was the walking locomotion. This locomotion was achieved through a three-step cycle[1] (Figure 6a and Video S4). First, the direction of B was fixed at $\alpha = 150°$, while B increased linearly until it peaked at $B_{max} = 10$ mT. Concurrently, the robot first anchored on its front end by frictional force and horizontal component of adhesive force and started to tilt forward. Second, the direction of B changed linearly from $\alpha = 150°$ to $\alpha = 120°$, while maintaining B at 10 mT. As a result, the robot posed a "C" shape. Finally, the direction of B was fixed at $\alpha = 120°$ while its magnitude decreased linearly from 10 to 0 mT. Concomitantly, the robot extended its front end, allowing it to make a net stride forward. Meanwhile, it anchored on its back end, also by frictional force as well as horizontal component of adhesive force. Such three steps mentioned above made up a whole walking cycle (Figure S11).

p-Si doping could effectively improve the walking locomotion under the circumstances of relatively small friction

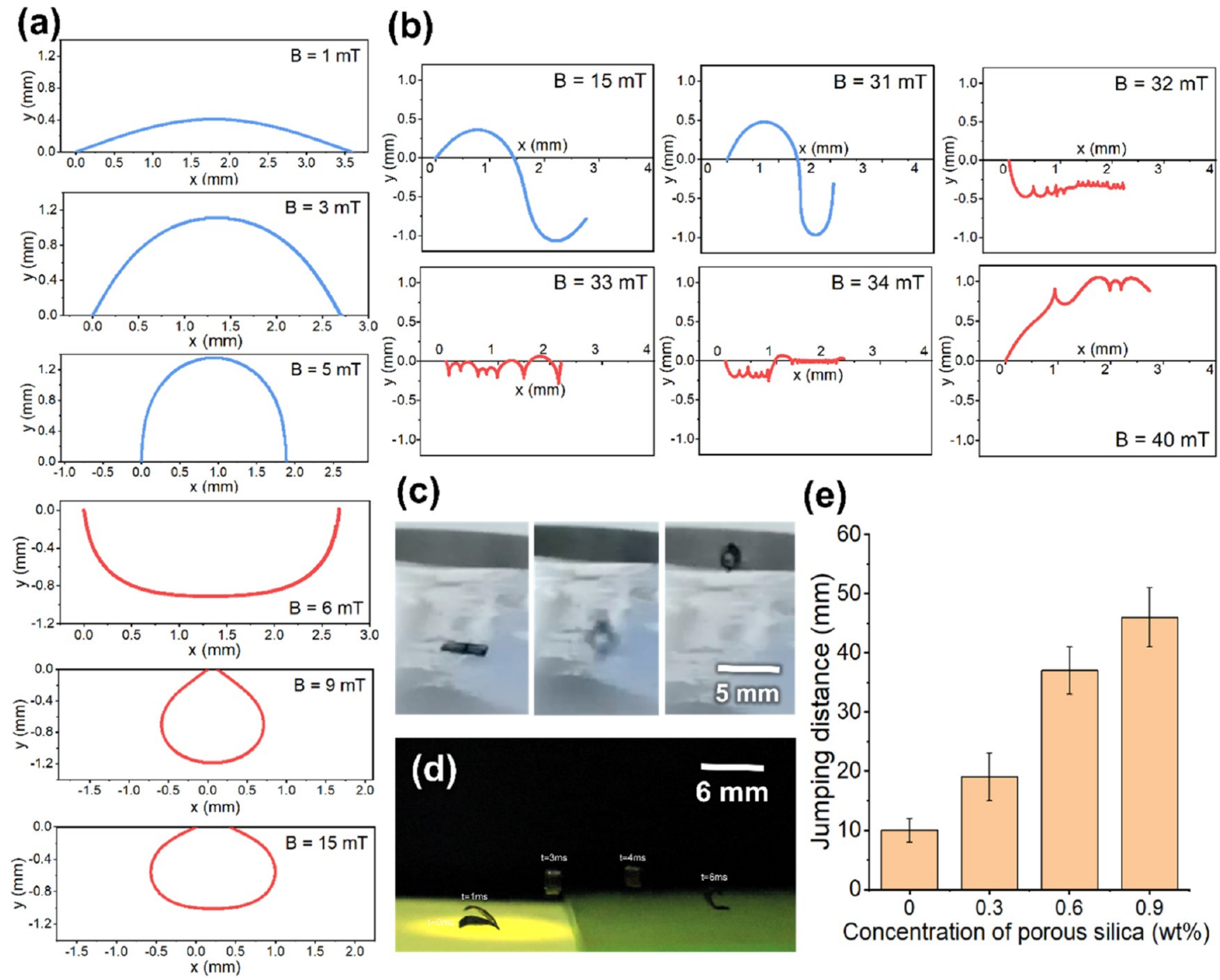

Figure 7. Analysis for jumping locomotion, including vertical jumping and horizontal jumping. (a) Deflection curves of the robot body in different magnitudes of magnetic fields (1, 3, 5, 6, 9, and 15 mT) for vertical jumping locomotion, showing the mechanism of vertical jumping. (b) Deflection curves of the robot body in different magnitudes of magnetic fields (15, 31, 32, 33, 34, and 40 mT) for horizontal jumping locomotion, showing the mechanism of horizontal jumping. (c) Captures showing the process of vertical jumping locomotion. (d) Captures showing the process of horizontal jumping locomotion. (e) Graph showing the relationship between p-Si concentration and horizontal jumping distance.

or large resistance, which was possibly attributed to enhanced adhesion. During the whole cycle, frictional and adhesive forces were indispensable. Without them, the robot would have bounced backward, resulting in its inability to march. Similar to previous analysis, adhesion would help with the walking locomotion, especially under the circumstances of a relatively small frictional force or large resistance. In fact, there should be a lot of fluid rushing in the human environment, which would cause great resistance to the walking locomotion of the microrobot. According to the analysis mentioned above, adhesion was the key to resist adverse current and maintain walking locomotion. Under certain variables, the upper limit of adhesion determined the maximum resistance that the robot could resist. Also, p-Si doping could effectively increase the adhesion of microrobots to certain substrates, thus improving the stability of walking locomotion. Three groups of experiments were conducted to verify the abovementioned theory.

First, oleic acid was added to the surface of weighing paper to construct a substrate with relatively little friction for walking locomotion. Robots walked at different speeds with different concentrations of doped p-Si (Figure 6b). Those with higher concentration had a larger adhesive force, which helped the robot to anchor its ends alternately, thus making a bigger stride in each cycle. Especially, walking locomotion was more sensitive to the lack of friction than rolling locomotion, as reflected in the more significant difference of walking speed among robots with various concentrations of p-Si doping. Also, the robot without doped p-Si almost marched on the spot (Figure 6b). This was because during walking locomotion, the contact area between the robot and the substrate was limited, so the adhesive force was deficient. This illustrated two points: adhesion was more decisive than friction; antiresistance walking locomotion required material improvement on adhesion.

The following two experiments focused on the increase in resistance. The second experiment was setting up resistance with a slope. A slope was built to change the effect of gravity on robots' walking locomotion. Referring to the previous force analysis of rolling locomotion (Figure 5c), increased resistance mainly consisted of the component of gravity parallel to the moving direction. In the experiment, three different materials were used as the substrate of the slope. Material type of substrate and concentration of p-Si doping were treated as two variables, and the process of robot walking on a slope was divided into three categories: reaching the top, almost reaching the top, and slipping half-way. A color block diagram was drawn to show the effect of walking locomotion in different situations (Figure 5c). Since walking locomotion was more sensitive to resistance than rolling, the angle of 10° was chosen as the slope angle instead of other higher degrees and apparent differences among testing samples could be obtained. The results correspond well to expectation: the greater the adhesion between the microrobot and substrate material, the better the walking locomotion stability. Also, it could effectively improve robots' walking locomotion on a slope by p-Si doping.

The third experiment was setting up resistance with wind. A tiny fan was set to blow in the forward direction of walking locomotion, increasing its wind force at a constant speed with the time gradient (three gears in total). A piece of cloth was strung to reflect the wind force. The air flow caused great disturbance to microrobot walking locomotion, which simulated some sudden changes in air pressure and hydraulic pressure in the human environment. Similarly, the experiment took the material type of substrate and p-Si concentration as two variables and divided the process of robot walking in the wind into three categories: successfully (reaching the end without pause and shaking), strugglingly (slight pausing or shaking, but still reaching the end), and unsuccessfully (pausing or even being blown away). A lattice diagram was drawn to show the stability of walking locomotion when encountering wind blowing (Figure 6d), taking the concentration of doped p-Si as the abscissa and the material type of substrate as the ordinate. The results were in line with expectation: the greater the adhesion between the robot and the substrate material, the better the walking locomotion. It could be explained that adequate adhesion force kept the end of the robot well-fixed on the substrate, even facing large disturbance (wind blowing).

Based on the three experiments mentioned above, it could be concluded that p-Si doping promoted walking locomotion by improving the adhesion of the robot body to substrate material, particularly when encountering deficient frictional force or obvious resistance. Since walking locomotion was another important way of marching, such results further proved that p-Si doping was greatly beneficial for the stability-enhanced marching of microrobots because increased adhesion caused by p-Si doping was needed for both rolling and walking locomotions.

Additionally, magnetic field setting of walking could realize the robot's drifting locomotion on water, based on reaction force provided by water and the fact that the surface tension of water was enough to allow the microrobot to float. The reaction of water provided the driving force, and the forward speed was obviously larger than that of walking. There were many gas−liquid and liquid−liquid two-phase surfaces in the human environment, where the drifting locomotion was useful. Also, the robot could achieve pulling and pushing actions on the water surface, breaking through obstacles ahead (Figure 6e). Moreover, microrobots could participate in the assembly of a magnetic-controlled boat which realized more complex functions, especially cargo delivery of larger volume (Video S5).

Jumping Locomotion: Vertical and Horizontal Jumping. Jumping locomotion was important for microrobots because during the moving process, apart from contacting with the substrate all the time, locomotions which could enable microrobots to move from one place directly to another place were also necessary.[25] In previous studies, leaps of robots often depended on complex mechanical drives.[26] For the magnetic soft microrobot, without complex mechanical devices, two kinds of jumping could be realized by different phase shift β, vertical jumping (Figure 7c, Video S6), and horizontal jumping (Figure 7d and Video S6). However, the jumping process for magnetic soft robots was still unclear, and jumping regulations were insufficient. Here, a physical model based on quasi-static analysis was raised to analyze the essence of jumping locomotion, and the effect of p-Si doping on jumping locomotion was explained in depth.

Vertical Jumping. According to mechanical analysis, the relationship between the rotation angle (θ) and deformation along the robot body (ds) could be expressed as given below

$$B_y \cos(\omega s + \beta + \theta) - B_x \sin(\omega s + \beta + \theta) = -\frac{EI_z}{Am}\frac{\partial^2\theta_{(s)}}{\partial s^2} \quad (1)$$

Along with boundary conditions, $\boldsymbol{M}_{\text{edge}} = 0$

$$\frac{\partial\theta_{(s)}}{\partial s}\Big|_{s=0} = \frac{\partial\theta_{(s)}}{\partial s}\Big|_{s=L} = 0 \quad (2)$$

When $\beta = -90°$, $B_x = 0$, and $B_y \neq 0$, the magnetic microrobot would perform vertical jumping locomotion. Different magnitudes of B_y were tried to get the corresponding deflection curves, from which the information about the mechanism of vertical jumping could be obtained (Figure 7a).

Since $\boldsymbol{M} = \boldsymbol{m} \times \boldsymbol{B}$, initially, the left part of the robot body had the tendency of counterclockwise rotation, while the right part had the tendency of clockwise rotation. This made the middle part go up, while two ends remain in touch with the substrate, forming a small deflection convex curve. If the small deflection convex curve accorded with the final stable shape, then the robot body would keep this shape on the substrate. However, if the deflection curve did not fit with the final stable shape, the robot body would undergo other kinds of deformation. When the deformation must occur but could not be accomplished relying on the support of the substrate, the robot would jump up.

According to calculation, when B_y was from 1 to 5 mT, the final stable shape was a small deflection convex curve (Figure 7a). Therefore, the robot body would just retain this stable shape on the substrate, never jumping up. In contrast, when B_y = 6 mT, the performance of solutions varied greatly, with the shape of the deflection curve changing from convex to concave. Therefore, the small deflection convex curve formed in the initial deformation was not stable, for the final state should be a concave curve with middle deflection. Therefore, the robot body had a tendency to convert to the expected final state. However, with the middle part of the robot body going up, the convex curved body could not turn to concave directly with the support of the flat substrate. Thus, it would continue to deform, accumulating elastic strain energy and kinetic energy while trying to reach the stable point but in fact went farther and finally jumped up at a certain point so as to release kinetic

https://doi.org/10.1021/acsami.1c25102
ACS Appl. Mater. Interfaces XXXX, XXX, XXX−XXX

energy and turn it to gravitational potential energy, achieving the high jump.

Nevertheless, the robot did not actually jump up when B_y = 6 mT, due to the fact that B_y = 6 mT was just near the critical point where the small deflection convex curve formed in the initial deformation turned to be unstable, so the driving force for jumping seemed too small. Since there were other impediments for the microrobot to jump up such as frictional energy loss, such small impetus would not induce the locomotion of vertical jumping. Instead, the initial B_y = 6 mT just counterbalanced the frictional energy loss (contact friction with the substrate, air drag, and viscoelastic losses within the soft robot), making the locomotion of jumping possible in a stronger magnetic field.

When B_y was from 6 to 9 mT, the degree of bending for stable deflection curve enhanced (Figure 7a), which did not change the tendency for the robot to jump up while enhancing the impetus. When B_y was larger than 9 mT, the stable deflection curve did not change apparently. However, larger magnitude of the magnetic field still provided more impetus for the locomotion of vertical jumping.

In the experiment, the lowest B_y for the soft robot body to jump up was 20.1 mT, which roughly equaled to the result of 18.9 mT in previous research. The magnitude of 20.1 mT accorded with our theoretical analysis above which 6 mT of magnetic field counterbalanced the frictional energy loss and provided the basic tendency for the robot to jump up, while higher magnitude of the magnetic field provided more impetus for the locomotion of jumping up. In our experiment, approximately 14.1 mT of magnetic field was used to provide additional impetus (could be seen as kinetic energy) for jumping up.

According to the analysis for the jumping mechanism, straight jumping height could be estimated from the perspective of energy conservation. The initial state was defined as the state where the robot body lay flat and still on the substrate, and the jumping critical state was defined as the state where the robot would jump up with a little bit more magnitude of the magnetic field. Based on the principle of energy conservation, between the two states, the soft robot gained energy from the work done by magnetic torque W. This energy was then redistributed into three components: the change in strain energy ΔS, kinetic energy ΔK, and frictional losses Q, during the jumping process.[1] Namely

$$W - \Delta S - Q = \Delta K \tag{3}$$

For the experiment, 6 mT of magnetic field provided the basic tendency for the robot to jump up, compensating for the energy loss, while approximately 14.1 mT of magnetic field was used to provide additional impetus for jumping up. The process could be simplified by making an assumption that the magnetic torque W caused by the initial 6 mT of magnetic field all turned into frictional losses Q, which became the basic tendency for the robot to jump up. Then, the other part of magnetic torque W caused by the sequential 14.1 mT of magnetic field turned into three parts—strain energy ΔS, kinetic energy ΔK, and frictional losses Q. The frictional losses Q equaled to half of magnetic torque W in this part, just as an object accelerated by a conveyor belt, only half of energy made the object to accelerate while another half became frictional losses.

At the maximum height, it was assumed that all the kinetic energy ΔK was fully converted into gravitational potential energy. Therefore

$$\Delta K = m_r g H_{max} \tag{4}$$

where m_r represented the mass of the robot.

Assume that the stable state of the 5 mT situation was roughly the shape of the robot body at the critical jumping point, after calculation (Text S4 for more detailed analysis)

$$H_{max} = 12.3 \text{ mm} \tag{5}$$

This result seemed to be a smaller approximation compared with the H_{max} given by previous research, which gave the theoretical calculation value of 25.9 mm. However, it should be noticed that the actual jumping height was always lower than theoretical results, with 6.8 mm in our experiment and 4.9 mm in previous studies[1]. Therefore, in our research, the theoretical result was much closer to the real jumping height in the experiment, giving a more accurate approximation. This proved the assumption that the stable state of the 5 mT situation was roughly the shape of the robot body at the critical jumping point was reasonable. Although the relative error was still non-negligible, but due to the fact that the measurement and calculation were complicated for soft robots that a lot of approximation should be introduced, and pervious research only showed higher relative error, our research had made significant improvements.

Horizontal Jumping. In the process of vertical jumping, the forces on the left and right side of the robot body were symmetric. However, in order to achieve horizontal jumping, another appropriate β should be set so that one side could move first. According to rational design, horizontal jumping could be achieved when $\beta = 0°$ and $B_x = 0$.

The basic equation could be expressed as

$$B_y \cos(1698.16s + \theta) = -3.91 \times 10^{-9} \frac{\partial^2 \theta_{(s)}}{\partial s^2} \tag{6}$$

Similarly, different B_y were tried and the corresponding deflection curves were achieved, from which information about the mechanism of horizontal jumping could be obtained (Figure 7b).

When magnetic field with y direction was provided, the left part and right part of the soft robot body had the tendency of counterclockwise rotation. In the same way, if the small deflection convex curve conformed to the final stable shape, the robot body would hold that shape on the substrate. However, if the small deflection convex curve did not conform to the final stable shape, other types of deformation might occur.

According to the results, when B_y < 32 mT, the final stable shape was only a smooth curve with small deflection, which was convex and had a counterclockwise movement trend for the left part (Figure 7b). Therefore, the robot body tended to stay in a stable state and did not jump up, achieving accumulation of elastic strain energy and kinetic energy during the process. However, when B_y = 32 mT, the stable state showed a sudden change (Figure 7b). The shape of the deflection curve on the left side changed from convex to concave, and the movement trend changed from counter-clockwise to clockwise. However, at this point, direct shape change could not occur. Thus, the deformation on the left would continue until it finally left the substrate at some point

https://doi.org/10.1021/acsami.1c25102
ACS Appl. Mater. Interfaces XXXX, XXX, XXX−XXX

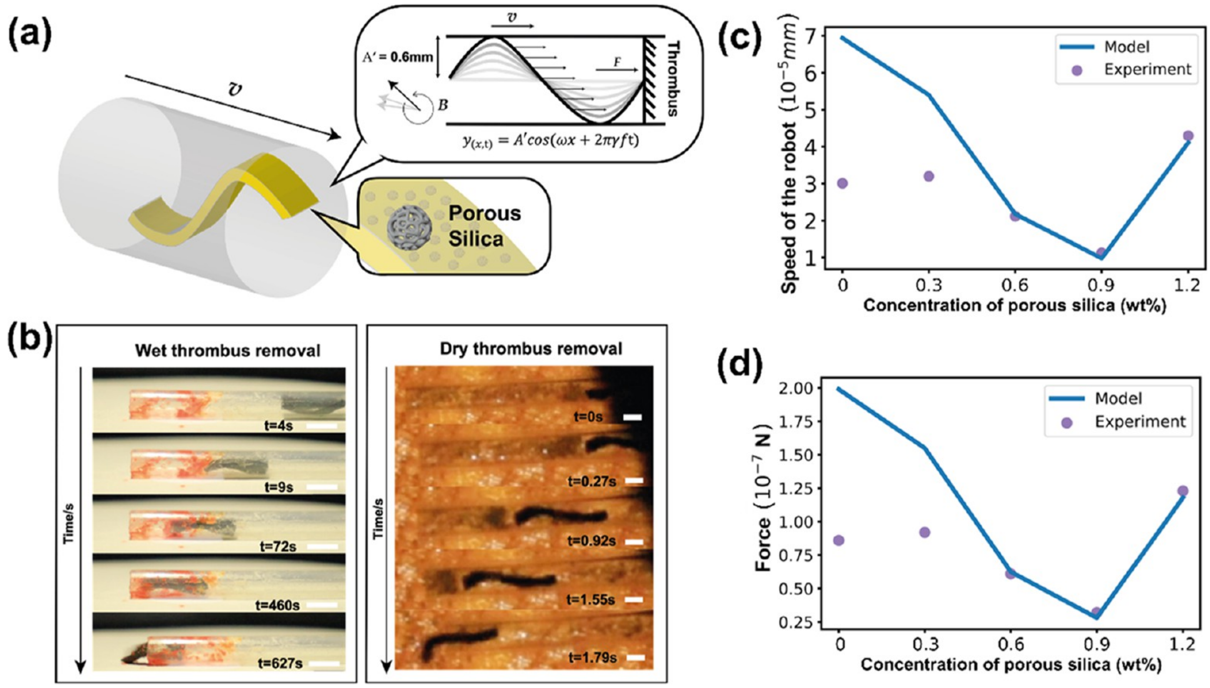

Figure 8. Schematic of crawling locomotion and thrombus removal. (a) Illustration of the crawling mechanism. (b) Demonstration of wet thrombus removal and dry thrombus removal. Scale bars, 5 mm for the left and 1 mm for the right. (c) Graph illustrating the relationship between crawling speed (pushing force) and p-Si doping concentration. (d) Graph illustrating the relationship between pushing force and p-Si doping concentration. In (c,d), theoretical results and experimental results were shown simultaneously.

and flipped to the right, where kinetic energy and elastic strain energy were converted into gravitational potential energy, achieving horizontal jump.

In the actual process, B_y = 32 mT was not the critical state for real jump due to the influence of frictional resistance. When B_y > 32 mT, the increase in magnetic field strength enhanced the accumulated energy, thus providing more power for jumping locomotion.

Effect of p-Si Doping Concentration on Jumping Locomotion. p-Si doping had a significant effect on jumping locomotion. Since experimental uncertainty was obvious for vertical jumping locomotion, it was more meaningful to analyze the relationship between p-Si doing concentration and horizontal jumping distance instead of vertical jumping height.

By comparing the jumping distance of microrobots with different p-Si doping concentrations, it could be found that with the increase in p-Si doping concentration (from 0 to 0.9 wt %), the horizontal jumping distance increased (Figure 7e). Namely, the horizontal jumping performance was improved by p-Si.

As was mentioned, the doping of p-Si had an effect on the mechanical properties of the robot body. With the increase in p-Si doping concentration (from 0 to 0.9 wt %), the elastic modulus decreased. According to analysis mentioned above, the jumping locomotion was a turning process from elastic strain energy to gravitational potential energy. Under the same magnetic field strength, robots with different p-Si doping concentration accumulated different elastic strain energy under the same bending degree. When the concentration was 0.9 wt %, the elastic modulus was the smallest and jumping distance was the longest. Therefore, the essence of the effect of p-Si doping concentration on jumping locomotion was that the change in the elastic modulus caused by variable p-Si doping concentration could affect the horizontal jumping distance.

Then, the impact of elastic modulus E on jumping distance was quantitatively analyzed from the perspective of energy conservation. Similar to vertical jumping, the transformation of magnetic torque W to strain energy ΔS, kinetic energy ΔK, and friction loss Q was also carried out in the process of horizontal jumping (eq 3).

In order to simplify the process, it was assumed that friction loss during the horizontal jumping process with different p-Si doping concentrations was the same. Since the motion trajectories of different microrobots were basically the same, this hypothesis could be considered reasonable. For strain energy ΔS, the expression had previously been derived as eq 11. Therefore, as E decreased, strain energy ΔS also decreased. Under the same magnetic moment, the larger the portion of energy converted to kinetic energy ΔK, the greater the initial velocity of jumping, resulting in a longer jumping distance. This was consistent with experimental results.

Therefore, p-Si doping had a beneficial effect on possible practical applications of microrobots by enhancing the horizontal jumping distance. Namely, microrobots with p-Si doping could achieve farther places due to softer body and higher flexibility, which indicated that they might accommodate better to a complex environment using jumping locomotion when the surroundings were not suitable for walking or rolling.

Crawling Locomotion and Thrombus Removal. For practical applications, microrobots should not only move on a surface but also move in a confined space, such as fine pipes in chemical reactors and animal blood vessels.[27] In such an environment, microrobots could not travel freely, and the corresponding locomotion must be realized by collision with the side wall. A direct idea was that if a periodic rotating magnetic field was applied, the robot could hit the pipe wall periodically, so it was possible to move forward continuously

https://doi.org/10.1021/acsami.1c25102
ACS Appl. Mater. Interfaces XXXX, XXX, XXX−XXX

with a cosine shape (Figure 8a,b and Video S7). This was similar to the locomotion of undulating swimming.[28] However, swimming was just an analogy, which could not be directly used to analyze crawling locomotion due to significant differences under boundary conditions. For the crawling of magnetic soft microrobots, previous studies only gave a fitting modal instead of clarifying the physical mechanism.[1] Here, a physical model based on analogy to mechanical waves was raised to get closer to the essence of crawling locomotion, and the effect of p-Si doping on crawling locomotion was explained in depth. Moreover, demonstration of thrombus removal was conducted to indicate application prospects of crawling locomotion, and p-Si doping might provide stronger impetus for thrombus removal.

Analysis of the Crawling Mechanism. According to the general theory, small deformation of microrobots could be expressed as

$$y_{(x)} = \frac{mBS}{EI_z\omega^3}\cos\,\omega x,\ 0 < x < L \tag{7}$$

In the crawling process, at any fixed time, the microrobot showed the shape of a cosine wave function (Figure 8b, Video S7), just like the mathematic relationship given in eq 9. However, considering time as another variable, the crawling locomotion did not work like either a normal travelling wave or a normal standing wave, instead, somewhere in between (Text S5 for more detailed analysis). Meanwhile, the amplitude $=\frac{mBS}{EI_z\omega^3}$, which was only suitable in free propagation, became no longer feasible owing to the boundary of the glass tunnel. Therefore, in order to describe the crawling locomotion, a new amplitude $A' = 0.6$ mm should be adopted, which was the radius of the glass tunnel. Thus, the wave function describing crawling locomotion could be expressed as

$$y_{(x,t)} = A'\cos(\omega x + 2\pi\gamma f t),\ 0 < x < L \tag{8}$$

γ is a damping coefficient that implied how the propagation of waves was influenced by the tube wall, f is the wave frequency, which equaled to the frequency of the applied rotating magnetic field. The influence of gravity was negligible in this case. To obtain the value of γ, the free amplitude A should be calculated first, by substituting $m = 77500$ A·m^{-1}, $B = 0.020$ T, $S = wh = 2.78 \times 10^{-7}$ m^2, $E = 9.30 \times 10^4$ Pa, $I_z = 7.91 \times 10^{-16}$ m^4, and $L = 0.0037$ m. Thus

$$A = \frac{mBS}{EI_z\omega^3} = \frac{mBSL^3}{8EI_z\pi^3} = 1.20 \times 10^{-3}\ \text{m} \tag{9}$$

Then, the coefficient γ could be expressed as the cubic of the ratio of bounded amplitude and free amplitude

$$\gamma = \left(\frac{A'}{A}\right)^3 = 0.125 \tag{10}$$

Since the robot body was seen as a whole period and wavelength λ was just microrobot body length L, the speed of robot v equaled to the wave speed u. Considering the phase propagation delay coefficient γ, the actual speed of microrobots could be expressed as

$$v = \gamma L f \tag{11}$$

Substituting = 0.50, $L = 3.7$ mm, and $f = 15$ Hz, it could be calculated that

$$v = 6.94\ \text{mm}\cdot\text{s}^{-1} \tag{12}$$

The speed of the microrobot v indicated how the robot crawled in a glass tunnel with a rotating magnetic field.

Effect of p-Si Doping Concentration on Crawling Locomotion. By doping different concentrations of p-Si in the robot body, the corresponding Young's modulus could be obtained by tensile test (Figure 3h). For the doping concentration of 0, 0.3, 0.6, 0.9, and 1.2 wt %, the calculated speed of the robot body v in the same rotating magnetic field was 6.94, 5.40, 2.18, 0.98, and 4.11 mm·s^{-1}, respectively (Figure 8c), which roughly conformed to the experimental results (3.01, 3.20, 2.12, 1.13, and 4.30 mm·s^{-1}, respectively, lower than expectation at 0 and 0.3 wt % due to low friction-induced slippery without enough p-Si doping). Hence, the crawling speed of the robot body had a trend of decreasing–increasing with the increase in p-Si doping concentration, which meant that different p-Si concentrations could be chosen for different needs for crawling speed. For maximum speed, 1.2 wt % concentration turned to be the best. For minimum speed, 0.6−0.9 wt % concentration was proper. 0−0.3 wt % concentration was not suitable for crawling because of low friction-induced slippery, which further proved that p-Si doping could enhance locomotion stability by enhanced adhesion to the substrate.

Application of Crawling Locomotion. Crawling locomotion was promising for minimally invasive surgery, and the application in surgical thrombectomy was remarkable. Blood circulates normally in the bloodstream but in some cases, blood might clump to form thrombus, as known as blood clots. Having life-threatening blood clots in the body might block the blood vessels, arteries, and veins, causing angiemphraxis, which might suddenly take away a human's life without any signals. Having a thrombectomy was the only way but there were a few risks that the patient might face such as excessive bleeding, permanent damage in blood vessels, and pulmonary embolism.[29] Hence, a minimally invasive way should be adopted and a microrobot with crawling locomotion was a representative example (Figure 8b and Video S7). The images below illustrated the whole process of thrombus removal. The wet thrombus and dry thrombus were experimented, respectively. In the wet thrombus case, a microrobot was put in a glass tunnel with radius $r = 0.6$ mm. From $t = 4$ s to $t = 9$ s, the robot crawled forward and met the wet bionic thrombus. From $t = 9$ s to $t = 627$ s, the robot successfully pushed away the thrombus and crawled over the glass tunnel. In the dry thrombus case, the robot could finish the task in 1.70 s, which was significantly faster than the wet case comparatively. By doping different amounts of p-Si, the corresponding forces that the microrobot push the thrombus could be calculated by the momentum theorem

$$Ft = mv \tag{13}$$

t is time of interaction, m is the mass of a microrobot, and v is the speed of crawling. It was noteworthy that t equaled to the period T because it could be assumed that the robot body would completely stop after each collision, which was reciprocal of frequency f. Hence

$$F = mvf \tag{14}$$

By substituting the mass $m = 1.91 \times 10^{-6}$ kg and frequency $f = 15$ Hz, the corresponding forces that microrobots doped by p-Si of 0, 0.3, 0.6, 0.9, and 1.2 wt % interacted with the thrombus could be obtained as 1.99×10^{-7}, 1.55×10^{-7}, 0.625

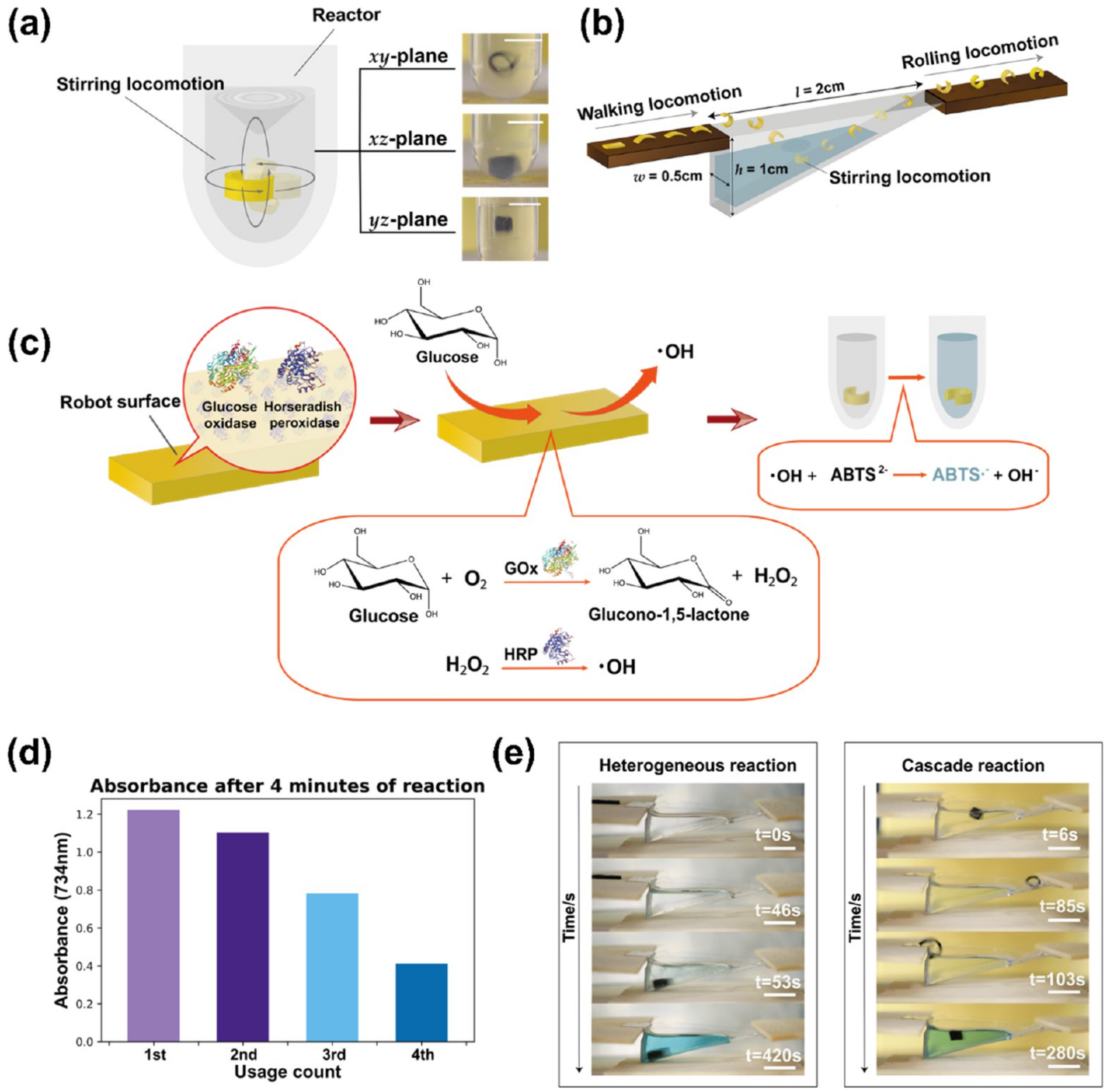

Figure 9. Schematic and data graph of stirring locomotion and biocatalysis. (a) Illustration of the stirring locomotion. Scale bars, 0.5 cm. (b) Illustration of the intelligent microchemical engineering system. (c) Illustration of the enzyme-carrying microrobots for biocatalysis, namely, the GOx−HRP cascade reaction. (d) Graph showing the relationship between usage times and absorbance after 4 min of reaction, showing the renewability of the enzyme-carrying microrobot. (e) Captures showing the process of the heterogeneous biocatalysis reaction and cascade biocatalysis reaction controlled by stirring locomotion of microrobots in the intelligent microchemical engineering system. Scale bars, 0.8 cm.

$\times 10^{-7}$, 0.281×10^{-7}, and 1.18×10^{-7} N, respectively (Figure 8d), which roughly conformed to the experimental results (0.862×10^{-7}, 0.917×10^{-7}, 0.607×10^{-7}, 0.324×10^{-7}, and 1.23×10^{-7} N, respectively, lower than expectation at 0 and 0.3 wt % due to low friction-induced slippery without enough p-Si doping). Hence, the pushing force of microrobots had a trend of decreasing−increasing with the increase in p-Si doping concentration, which meant that different p-Si concentrations could be chosen for different needs for thrombus removal. For maximum force, 1.2 wt % concentration turned to be the best. For minimum force, 0.6−0.9 wt % concentration was proper. 0−0.3 wt % concentration was not suitable for crawling because of low friction-induced slippery, which further proved that p-Si doping could enhance locomotion stability by enhancing adhesion to the substrate. In most cases, a force large enough was needed for thrombus removal; then, 1.2 wt % concentration would be a proper choice.

In summary, the crawling locomotion of magnetic soft microrobots was clarified in this study. The essence of crawling could be seen as mechanical waves with phase propagation delay due to pipe wall constraints. Flexibility was very important for motion under boundary constraints, which highlighted the significance of p-Si doping. Microrobots doped with 1.2 wt % p-Si could move the most smoothly in a tube and had potential for thrombus removal due to relatively strong impact force.

Stirring Locomotion and Biocatalysis. *Stirring Mechanism.* By applying a rotating magnetic field with three axes alternating (Figure 9a), the robot stirred the solution steadily (Video S8). The mechanism of stirring locomotion was similar to rolling locomotion, in other words, rolling in the liquid

https://doi.org/10.1021/acsami.1c25102
ACS Appl. Mater. Interfaces XXXX, XXX, XXX−XXX

environment. Stirring locomotion could highly increase the rate of reaction as it could make reactants mix more intensively.[30] Compared with a normal magnetic stirrer, microrobots could be made into any size conveniently, and its soft body made it perform adaptive locomotion[31] not to be stopped by hitting the container wall but showed stronger stirring effect by circulating along the container wall instead. From this perspective, the p-Si doping concentrations which could soften the robot body would contribute to stirring locomotion, enhancing locomotion stability by promoting its adaptive locomotion.

Owing to the features of the robot-like small dimension and magnetic control, it was promising for organizing an intelligent microreactor (Figure 9b). The model was assembled by a wooden platform and plastic container. The robot could walk over the platform and jump into the container, which played a role of a reactor. Then, the robot started stirring and rolled away after finishing the task (Video S8). Using this combination of walking, stirring, and rolling locomotion, an efficient and effective intelligent microreactor was achieved. Such an intelligent microreactor could proceed a reaction automatically without touching the reactants inside, contributing to the remote control of chemical reactions[32] and optimization of reaction conditions.[33]

Applications on Intelligent Microreactor and Biocatalysis. Meanwhile, there was also a promising application in biocatalysis by microrobots loading various enzymes. Enzyme loading was an important direction for biocatalysis because it could greatly facilitate targeted catalysis[34] and enzyme recycling.[35] Enzyme-loading microrobots could work as catalysts and magnetic stirrers at the same time, enhancing the reaction rate by two mechanisms together. The glucose oxidase (GOx) and horseradish peroxidase (HRP) cascade reaction was taken as an example, which had prospects for cancer starvation therapy[36] and high-throughput detection of blood glucose.[37] Glucose was oxidized to gluconic acid with the catalysis of GOx and forming H_2O_2 which would be decomposed into two hydroxyl radicals. Eventually, hydroxyl radicals would react with 2,2'-azinobis-(3-ethylbenzothiazoline-6-sulfonic acid) (ABTS), forming $ABTS^{-\bullet}$ whose solutions presented blue color and characteristic absorbance was between 400 and 430 nm.[38] Two different enzymes catalyzed two consecutive steps of reaction, with blue color occurring in the final step (Figure 9c). In this research, GOx and HRP were loaded in the base material of microrobots. After magnetization, the enzyme-loaded robot was put into a solution with glucose and ABTS in a rotating magnetic field. After a few seconds, the solution significantly turned blue, verifying the catalysis effect of enzyme-loading microrobots.

Moreover, the enzyme-loading microrobots had good performance in renewability after using an abrasive paper to rub the robot surface (Figure 9d). From the first usage to the fourth usage, the average reaction rate from $t = 0$ s to $t = 240$ s was 1.19×10^{-4}, 1.03×10^{-4}, 6.70×10^{-5}, and 2.19×10^{-5} $mmol \cdot L^{-1} \cdot s^{-1}$, respectively, which revealed that the enzyme-carrying robots still had significant biocatalysis properties after repeated use.

A stirring microrobot was also beneficial in heterogeneous reactions (Figure 9e). At $t = 0$ s, 20 μL of mixed enzyme aqueous solution containing GOx and HRP was added, which floated on the surface of glucose–ABTS–glycol (50%) mixed solution, forming a phase interface with blue color.[39] The moving of the phase interface was extremely slow with significant movement after 53 s, which greatly limited the reaction rate. However, when stirring locomotion was triggered, reactants were immediately mixed fully so the reaction could proceed smoothly.

Controlling the process of reaction was also an essential part because it was necessary to make reactions proceed stepwise and controllable. The GOx–HRP cascade reaction could be set as a representative example via controlling stepwise. By loading GOx and HRP in two microrobots, respectively, the stepwise reaction could be achieved automatically (Figure 9e and Video S8). First, the robot loaded with GOx rolled into the reactor. After 79 s of stirring, the first robot rolled out and the first step of the GOx–HRP cascade reaction finished, forming H_2O_2. Then, the second robot loaded with HRP rolled in and began to stir; then, the solution started to turn blue gradually, which was the second step of the GOx–HRP cascade reaction.

In summary, the stirring locomotion of magnetic soft microrobots, derived from rolling locomotion, could work as flexible magnetic stirrers. Since p-Si doping could enhance flexibility, microrobots doped with p-Si stirred in a confined container more smoothly. Apart from stirring, microrobots could also carry enzymes for targeted biocatalysis. Combined with multimodal locomotion, such a microrobot could contribute to the core of an intelligent microreactor, realizing remote and automatic control of chemical reactions.

Simulation of Multimodal Locomotion *in Vivo*. To illustrate the robot's ability to actualize multimodal locomotions and tasks assigned in a real situation, microrobots were put under a simulated in vivo environment (Video S9). In order to fully explore the robot's potential at realistic significance, representative organ models in the surgical process were selected as the background environment: human stomach (Figure 10a,b) and blood vessel (Figure 10c,d). In accordance to the realistic anatomical situation

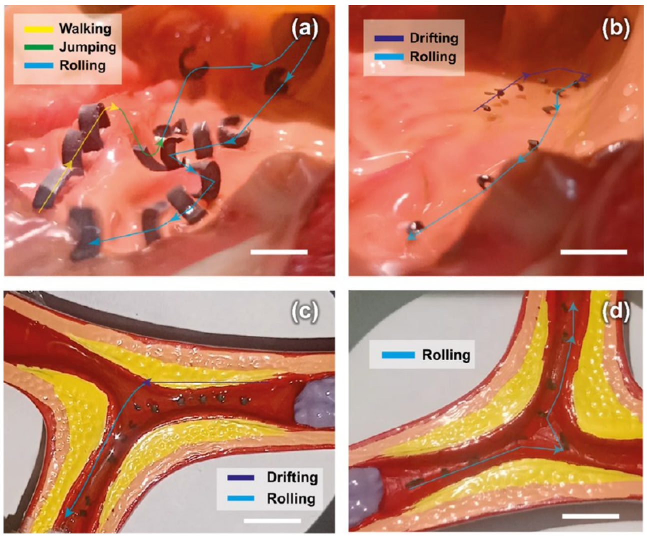

Figure 10. Simulation of multimodal locomotion in vivo. (a) Simulation of multimodal locomotion in a human stomach, solid environment. Scale bar, 8 mm. (b) Simulation of multimodal locomotion in a human stomach, watery environment. Scale bar, 8 mm. (c) Simulation of multimodal locomotion in blood vessels, watery environment. Scale bar, 2 cm. (d) Simulation of multimodal locomotion in blood vessels, solid environment. Scale bar, 2 cm.

https://doi.org/10.1021/acsami.1c25102
ACS Appl. Mater. Interfaces XXXX, XXX, XXX–XXX

where the body fluid was randomly distributed in an organ, both conditions as of with and without fluid were simulated.

The robots performed different combinations of motions in response to different environments. On rugged paths such as in the stomach, a complex combination of modes of motions was applied in order to overcome the obstacles. In addition, compared to the watery environment, the waterless path had more resistance to movement. A varied multimodal series of motion (including walking, jumping, and rolling), therefore, was required to go over the dynamic barrier of the randomly protruding surfaces (Figure 10a). During the walking locomotion, the robot tilted its gravity center and extended its front leg across the low-height wrinkled surface to go forth. By shifting anchorage back and forth, it came across the mildly rugged surface. When the robot met the barrier of greater height, the magnetic field was adjusted to induce shape deformation and rigid body rotation so that the robot jumped over the high barrier. On a relatively smooth terrain, *B* rotated clockwise to produce rolling locomotion, increasing the efficiency of movement.

On the watery surface where less obstacles on the forwarding path were present, the robot moved with more suitable multimodal locomotion: drifting and rolling (Figure 10b). The surface tension of liquid supported the robot's movement, allowing it to stand and walk on the water surface. With basic locomotion similar to walking but on the fluid surface, the robot drifted off at relatively high speed. The robot could also roll in the watery environment, which was at high efficiency of delivery as well. *B* changed into a rotating magnetic field, bending the robot to a circular curved shape that allowed for rolling. As it started with the rolling locomotion, which generated greater disturbance to the environment, surface tension was no longer capable of supporting its motion on the surface. The robot, thus, started rolling at the solid base of the environment.

As the environment was relatively uniform in simulated blood vessels, a simpler combination of motion was applied. With steady surface and little obstacles on the path, a rotating *B* was applied to induce rolling locomotion for higher efficiency of delivery (Figure 10d). By adjustment of the magnetic field rotating plane, microrobots could turn in the rolling process so as to adapt to the complex bifurcation structure in blood vessels. Moreover, two locomotions (drifting and rolling) in the fluid-contained blood vessel model were realized together (Figure 10c), demonstrating the robot's ability to move both on and under the water surface. Both of these locomotions, controlled by the changing magnetic field, were effective transferring the method of high speed in a watery environment.

In order to simulate movement in blood vessels with greater consistency to reality, water current was applied in the scenario to demonstrate the body fluid with high fluidity (Video S9). The water currents were simulation of random body fluid flow. Under rotating *B*, the robot rolled back and forth over the created path where water flowed through, illustrating its ability to move steadily, mostly unaffected by the surrounding flow field. In addition, the simulation of muscle peristalsis was also realized, and the rolling locomotion could still take place in such an environment (Video S9).

From the simulation mentioned above, it was concluded that microrobots in this study had the potential for in vivo movement. p-Si doping enhanced microrobot locomotion stability by increasing adhesion and softening the robot body, thus enlightening the prospect of multimodal locomotion in a nonideal environment with great disturbance. Compared with previous research, this study contributed significant progress. For multitasking precision medicine, microrobots would certainly meet a lot of nonideal hindrance, which was not placed on a vital position for previous studies. However, no matter how sophisticated a single locomotion was, if it could not proceed normally in an actual working environment, then the design would be greatly limited for future use. In this study, every single locomotion was proved to have enhanced stability via p-Si doping, and they could still take place normally when combined together in a simulated in vivo environment with original and artificial hindrance. Thus, the prospect of magnetic soft microrobots for precision medicine became closer to reality.

■ CONCLUSIONS

In conclusion, a p-Si-doped flexible magnetic microrobot for enhanced stability of multimodal locomotion in a nonideal biological environment was demonstrated in this study (Figure 11). The doping of p-Si not only improved adhesion properties but also refined comprehensive mechanical properties of the microrobot. On the basis of fundamental locomotions including rolling, walking, jumping, and crawling and complex locomotions combined by basic motions via rational design

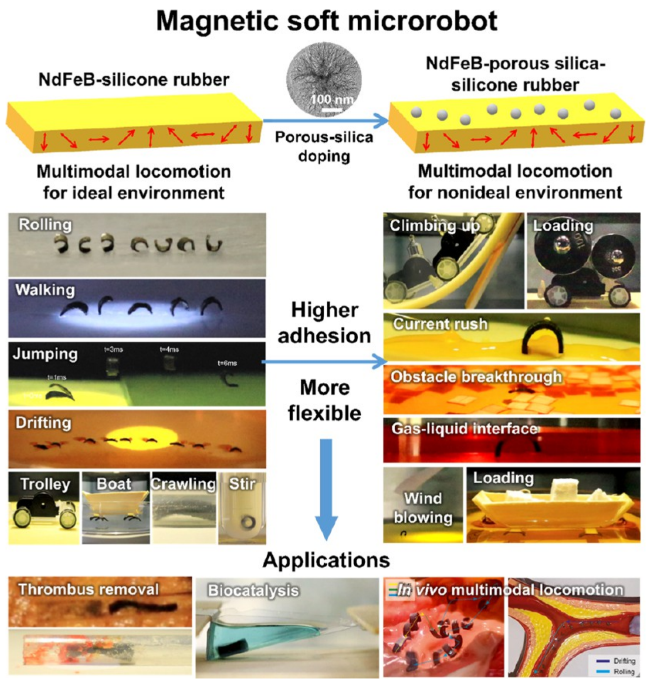

Figure 11. Summary figure, an overall illustration of the p-Si-doped soft magnetic microrobot for enhanced stability of multimodal locomotion in a nonideal biological environment. In previous studies, magnetic soft microrobots made of NdFeB−silicone rubber could achieve multimodal locomotion only in an ideal environment. In this research, after p-Si doping, the upgraded microrobot made of NdFeB−p-Si−silicone rubber had more adhesion and become more flexible so as to achieve multimodal locomotion successfully for a nonideal environment, such as climbing up, loading, current rush, obstacle breakthrough, gas−liquid interface, and wind blowing. Such an upgrade provided promising prospects for practical applications of microrobots, including thrombus removal, biocatalysis, and in vivo targeted therapy.

including drifting, stirring, trolley, and boat, the influence of p-Si doping on stability of each locomotion in a nonideal environment was explored in depth, and p-Si doping turned out to be beneficial for stability enhancement of most locomotions. Different from previous locomotion demonstrations in an ideal environment, due to silica doping, motions in this study could be conducted in nonideal circumstances such as climbing, loading, current rushing, wind blowing, and obstacle hindering. Such a stability-enhanced multimodal locomotion system was used in biocatalysis and thrombus removal, and in vivo demonstration of multimodal locomotion with nonideal disturbance enlightened its prospect for precision medicine.

However, this study still has obvious limitations. Compared with previous research, this work has innovatively made an attempt to explore locomotion stability in a practical nonideal biological environment. However, since the concept of the nonideal biological environment itself is too complex to be explained by limited experiments, this work could only focus on some major kinds of disturbance that the microrobot may face in the human body; thus, relative results only indicate a theoretical feasibility instead of assuring the practicability in real medical application. Currently, the development of a magnetic soft microrobot is still at the state of beginning and in vivo experiment is hard to conduct (although appropriate simulation can be conducted) for the sake of safety and ethics.[40] After more demonstration for security, an in vivo experiment will be conducted to verify the feasibility of this p-Si-doped flexible magnetic microrobot for enhanced stability of multimodal locomotion in a nonideal biological environment, contributing to the future development of precision medicine and other related aspects.

EXPERIMENTAL SECTION

Chemicals. Triethanolamine (TEA), hexadecyl trimethyl ammonium bromide (CTAB), sodium salicylate (NaSal), tetraethyl orthosilicate (TEOS), diammonium ABTS, glucose, GOx, HRP, NdFeB magnetic microparticles, oleic acid, ethylene glycol, and ethanol were purchased from Sigma-Aldrich. The Ecoflex 00−10 polymer matrix was purchased from Smooth-On Inc. Silicone rubber, PU, and PTFE were purchased from DuPont Chemical Co., Ltd. Deionized water was purified using a Milli-Q system. All other chemicals were used as received.

Synthesis of Dendritic Mesoporous Silicon Nanoparticles. 60 μL of TEA was added to 25 mL of deionized water, and the mixture was shaken at 160 rpm in a water bath at 80 °C for 0.5 h. Then, 380 mg of CTAB and 168 mg of NaSal were added and continued shaking was applied for 1 h. Afterward, 4 mL of TEOS was added, and a continued shaking was applied for 2 h. Then, the mixture was centrifuged at 7000 rpm for 20 min to collect the products. The products were washed with ethanol three times to remove the residual reactants and finally dried overnight in vacuum at room temperature.

Preparation of Magnetic Soft Microrobots. The composition of the robot involved neodymium iron boron (NdFeB) magnetic microparticles (MQP 15-7, Magnequench; average diameter: 5 μm, density: 7.61 g·cm^{-3}), the Ecoflex 00−10 polymer matrix A and B (Smooth-On Inc.; density: 1.04 g·cm^{-3}), and p-Si microparticles. The amount of NdFeB, Ecoflex A, and Ecoflex B added for each glass slab was determined in correspondence to the thickness of the layer and area of the slab, and the amount of p-Si added was calculated through the demanded concentration of the material.

Two specifications were made for different uses throughout the experiment. The first specification created films of 1 mm. Slabs of approximately 100 cm^2 were used as a model for film construction. Ecoflex A (4.4 g) was added onto the glass slab first, and then, NdFeB microparticles (8.8 g) were added onto the polymer matrix Ecoflex A on slab in order to avoid dispersion to other places. p-Si microparticles were added in the calculation of concentration (e.g., the preset 0.2% concentration involved 0.0352 g of porous silicon micro-particles). Ecoflex B (4.4 g) was added at last, since it started to react with Ecoflex A to form cross-linking structure once added. The second specification created films of 0.2 mm, which involved a glass slab of 48 cm^2 and the addition of 1 g of NdFeB microparticles, 0.5 g of Ecoflex A, 0.5 g of Ecoflex B, and p-Si particles in correspondence to concentration.

After the addition of materials, the stirring glass rod was used to fully mix the mixture on the glass slab and to ensure that the film of uniform thickness was made. The uniformly mixed mixture was placed in the air for 5 h to solidify (Figure S12).

Measurements and Characterization. SEM images were recorded on a Zeiss Gemini high-resolution scanning electron microscope (Germany) operating at 5 kV. The EDS images were recorded while operating at 15 kV. Microrobot samples were first put into liquid nitrogen and then broke, leaving quenched sections for observation. TEM images were taken with a JEOL 2011 microscope (Japan) operated at 200 kV. Magnetic characterization was conducted on a vibrating sample magnetometer LakeShore 8604.

Magnetization of Magnetic Soft Microrobots. After solidification, the film was cut into pieces, becoming the robot bodies. The cutting involved two specifications, each corresponding to the specific thickness of the film. For films of 1 mm (h = 1 mm), each robot had dimensions of w = 3.6 mm and L = 8.9 mm; for films of 0.2 mm (h = 0.2 mm), each robot had dimensions of w = 1.5 mm and L = 3.7 mm.

The robot body of 8.9 mm length was then wrapped around a cylindrical wood rod with a circumference of 8.9 mm; the robot with 3.7 mm length was wrapped around a rod with 3.7 mm circumference. In order to receive uniform magnetization, the robots were vertically wrapped around the rod without any overlapping. The soft-bodied robots were then put into the pulse magnetizer (Beijing EUSCI Technology Limited), which could give a magnetic pulse of 2.5 T for magnetization. The angles by which robots were put into the magnetizer turned to be important, as it necessarily created a phase shift β in the magnetization profile m. It was determined by the angle between the vertical direction and the wrapping start point. After magnetization, the robot was unwrapped, and a harmonic magnetization profile was achieved.

Tensile Test and Tensile-Adhesion Test. Tensile test of materials containing different concentrations of p-Si was performed to directly reveal the mechanical properties of the synthesized material. The tensile test was performed at room temperature on a universal testing machine (SHIMADZU) with 50 N load cells. Samples of rectangular shape with a width of 10 mm, a length of 40 mm, and a height of 1 mm were used. The samples were placed between two platforms, with both ends gripped by the machine grips: upper in the moving grips and lower in the fixed grips. The rate of stretching was constantly 60 mm·min^{-1}. The mechanical parameters were calculated from the stress−strain curve.

With a similar method, properties of adhesion and toughness were also measured, which was called the tensile-adhesion test. The tensile-adhesion test was performed at room temperature on a universal testing machine (SHIMADZU) with 50 N load cells. To measure the property of adhesion, samples with a size of 37 mm in width, 38 mm in length, and 1 mm in height were used. The samples were presettled onto a flat horizontal square platform. The platform had a vertical handle for the testing machine to grip. As a whole, the device was T-shaped. The samples were placed between two platforms, with both handles gripped by the machine grips: upper in the moving grips and lower in the fixed grips. The rate of stretching was constantly 60 mm/min. The related parameters were calculated from the stress−strain curve.

Realization of Multimodal Locomotion. Details were listed in the Supporting Information.

https://doi.org/10.1021/acsami.1c25102
ACS Appl. Mater. Interfaces XXXX, XXX, XXX−XXX

■ ASSOCIATED CONTENT

Supporting Information

The Supporting Information is available free of charge at https://pubs.acs.org/doi/10.1021/acsami.1c25102.

Basic theory of magnetic microrobot locomotion and more details of experimental operations (PDF)
Tensile test (MP4)
Rolling (MP4)
Magnetically controlled trolley (MP4)
Walking (MP4)
Drifting and magnetically controlled boat (MP4)
Jumping (MP4)
Crawling and thrombus removal (MP4)
Stirring and biocatalysis (MP4)
In vivo simulation (MP4)

■ AUTHOR INFORMATION

Corresponding Author

Yuan Lu − *Key Laboratory of Industrial Biocatalysis, Ministry of Education, Department of Chemical Engineering, Tsinghua University, Beijing 100084, China*; orcid.org/0000-0003-4500-6230; Email: yuanlu@tsinghua.edu.cn

Authors

Shangsong Li − *Key Laboratory of Industrial Biocatalysis, Ministry of Education, Department of Chemical Engineering, Tsinghua University, Beijing 100084, China; School of Materials Science and Engineering, Tsinghua University, Beijing 100084, China*

Dong Liu − *Key Laboratory of Industrial Biocatalysis, Ministry of Education, Department of Chemical Engineering, Tsinghua University, Beijing 100084, China*

Yuping Hu − *Key Laboratory of Industrial Biocatalysis, Ministry of Education, Department of Chemical Engineering, Tsinghua University, Beijing 100084, China*

Zhijie Su − *Key Laboratory of Industrial Biocatalysis, Ministry of Education, Department of Chemical Engineering, Tsinghua University, Beijing 100084, China*

Xinai Zhang − *Key Laboratory of Industrial Biocatalysis, Ministry of Education, Department of Chemical Engineering, Tsinghua University, Beijing 100084, China; Beijing No.4 High School International Campus, Beijing 100034, China*

Ruirui Guo − *Key Laboratory of Industrial Biocatalysis, Ministry of Education, Department of Chemical Engineering, Tsinghua University, Beijing 100084, China; College of Bioengineering, Tianjin University of Science and Technology, Tianjin 300457, China*

Dan Li − *Key Laboratory of Industrial Biocatalysis, Ministry of Education, Department of Chemical Engineering, Tsinghua University, Beijing 100084, China*

Complete contact information is available at: https://pubs.acs.org/10.1021/acsami.1c25102

Author Contributions

S.L., D.L., and Y.H. contributed equally to this paper. S.L., D.L., and Y.L. proposed and designed the research. S.L., Y.H., Z.S., X.Z., D.L., and R.G. performed the experiments. S.L., Y.H., Z.S., and D.L. developed theoretical models. D.L., Y.L., and R.G. provided instructions on experimental design and paper writing. S.L., Y.H., Z.S., X.Z., and D.L. analyzed experimental data and wrote the paper. X.Z. finished video capture and editing. All authors participated in discussions.

Notes

The authors declare no competing financial interest.

■ ACKNOWLEDGMENTS

This work was supported by the National Key R&D Program of China (2018YFA0901700), the National Natural Science Foundation of China (21878173), and a grant from the Institute Guo Qiang, Tsinghua University (2019GQG1016).

■ REFERENCES

(1) Hu, W.; Lum, G. Z.; Mastrangeli, M.; Sitti, M. Small-scale soft-bodied robot with multimodal locomotion. *Nature* **2018**, *554*, 81−85.

(2) Nelson, B. J.; Kaliakatsos, I. K.; Abbott, J. J. Microrobots for Minimally Invasive Medicine. *Annu. Rev. Biomed. Eng.* **2010**, *12*, 55−85.

(3) Sitti, M.; Ceylan, H.; Hu, W.; Giltinan, J.; Turan, M.; Yim, S.; Diller, E. Biomedical Applications of Untethered Mobile Milli/Microrobots. *Proc. IEEE* **2015**, *103*, 205−224.

(4) Hoop, M.; Ribeiro, A. S.; Rösch, D.; Weinand, P.; Mendes, N.; Mushtaq, F.; Chen, X.-Z.; Shen, Y.; Pujante, C. F.; Puigmartí-Luis, J.; Paredes, J.; Nelson, B. J.; Pêgo, A. P.; Pané, S. Mobile Magnetic Nanocatalysts for Bioorthogonal Targeted Cancer Therapy. *Adv. Funct. Mater.* **2018**, *28*, 1705920.

(5) Lee, W.; Nam, J.; Kim, J.; Jung, E.; Jang, G. Effective Locomotion and Precise Unclogging Motion of an Untethered Flexible-Legged Magnetic Robot for Vascular Diseases. *IEEE Trans. Ind. Electron.* **2018**, *65*, 1388−1397.

(6) Erkoc, P.; Yasa, I. C.; Ceylan, H.; Yasa, O.; Alapan, Y.; Sitti, M. Mobile Microrobots for Active Therapeutic Delivery. *Adv. Ther.* **2019**, *2*, 1800064.

(7) Aguilar, J.; Zhang, T.; Qian, F.; Kingsbury, M.; McInroe, B.; Mazouchova, N.; Li, C.; Maladen, R.; Gong, C.; Travers, M.; Hatton, R. L.; Choset, H.; Umbanhowar, P. B.; Goldman, D. I. A review on locomotion robophysics: the study of movement at the intersection of robotics, soft matter and dynamical systems. *Rep. Prog. Phys.* **2016**, *79*, 110001.

(8) Ren, Z.; Hu, W.; Dong, X.; Sitti, M. Multi-functional soft-bodied jellyfish-like swimming. *Nat. Commun.* **2019**, *10*, 2703.

(9) Du, X.; Cui, H.; Xu, T.; Huang, C.; Wang, Y.; Zhao, Q.; Xu, Y.; Wu, X. Reconfiguration, Camouflage, and Color-Shifting for Bioinspired Adaptive Hydrogel-Based Millirobots. *Adv. Funct. Mater.* **2020**, *30*, 1909202.

(10) Chen, Y.; Wang, H.; Helbling, E. F.; Jafferis, N. T.; Zufferey, R.; Ong, A.; Ma, K.; Gravish, N.; Chirarattananon, P.; Kovac, M.; Wood, R. J. A biologically inspired, flapping-wing, hybrid aerial-aquatic microrobot. *Sci. Robot.* **2017**, *2*, No. eaao5619.

(11) Ye, Z.; Sitti, M. Dynamic trapping and two-dimensional transport of swimming microorganisms using a rotating magnetic microrobot. *Lab Chip* **2014**, *14*, 2177−2182.

(12) Zhu, Y.; Mottaghi, R.; Kolve, E.; Lim, J. J.; Gupta, A.; Fei-Fei, L.; Farhadi, A. Target-driven visual navigation in indoor scenes using deep reinforcement learning. *2017 IEEE International Conference on Robotics and Automation (ICRA), 29 May-3 June 2017*, 2017; pp 3357−3364.

(13) Shuai, J.; Sun, Y.; Tan, X.; Mori, T. Manipulating the Ge Vacancies and Ge Precipitates through Cr Doping for Realizing the High-Performance GeTe Thermoelectric Material. *Small* **2020**, *16*, 1906921.

(14) Choi, S.; Choi, Y. j.; Jang, M. S.; Lee, J. H.; Jeong, J. H.; Kim, J. Supertough Hybrid Hydrogels Consisting of a Polymer Double-Network and Mesoporous Silica Microrods for Mechanically Stimulated On-Demand Drug Delivery. *Adv. Funct. Mater.* **2017**, *27*, 1703826.

(15) Jung, H.; Kim, M. K.; Lee, J. Y.; Choi, S. W.; Kim, J. Adhesive Hydrogel Patch with Enhanced Strength and Adhesiveness to Skin for Transdermal Drug Delivery. *Adv. Funct. Mater.* **2020**, *30*, 2004407.

(16) Hu, X.; Nian, G.; Liang, X.; Wu, L.; Yin, T.; Lu, H.; Qu, S.; Yang, W. Adhesive Tough Magnetic Hydrogels with High Fe3O4 Content. *ACS Appl. Mater. Interfaces* **2019**, *11*, 10292−10300.

(17) Wang, S.; Xu, J.; Wang, W.; Wang, G.-J. N.; Rastak, R.; Molina-Lopez, F.; Chung, J. W.; Niu, S.; Feig, V. R.; Lopez, J.; Lei, T.; Kwon, S.-K.; Kim, Y.; Foudeh, A. M.; Ehrlich, A.; Gasperini, A.; Yun, Y.; Murmann, B.; Tok, J. B.-H.; Bao, Z. Skin electronics from scalable fabrication of an intrinsically stretchable transistor array. *Nature* **2018**, *555*, 83−88.

(18) Yang, Y.; Bernardi, S.; Song, H.; Zhang, J.; Yu, M.; Reid, J. C.; Strounina, E.; Searles, D. J.; Yu, C. Anion Assisted Synthesis of Large Pore Hollow Dendritic Mesoporous Organosilica Nanoparticles: Understanding the Composition Gradient. *Chem. Mater.* **2016**, *28*, 704−707.

(19) Sugibayashi, K.; Todo, H.; Oshizaka, T.; Owada, Y. Mathematical Model to Predict Skin Concentration of Drugs: Toward Utilization of Silicone Membrane to Predict Skin Concentration of Drugs as an Animal Testing Alternative. *Pharm. Res.* **2009**, *27*, 134.

(20) Akindoyo, J. O.; Beg, M. D. H.; Ghazali, S.; Islam, M. R.; Jeyaratnam, N.; Yuvaraj, A. R. Polyurethane types, synthesis and applications—a review. *RSC Adv.* **2016**, *6*, 114453−114482.

(21) Estermann, M.; Spiaggia, G.; Septiadi, D.; Dijkhoff, I. M.; Drasler, B.; Petri-Fink, A.; Rothen-Rutishauser, B. Design of Perfused PTFE Vessel-Like Constructs for In Vitro Applications. *Macromol. Biosci.* **2021**, *21*, 2100016.

(22) Pieters, R.; Tung, H.; Charreyron, S.; Sargent, D. F.; Nelson, B. J. RodBot: A rolling microrobot for micromanipulation. *2015 IEEE International Conference on Robotics and Automation (ICRA), 26−30 May 2015*, 2015; pp 4042−4047.

(23) Chung, F. H. Unified theory and guidelines on adhesion. *J. Appl. Polym. Sci.* **1991**, *42*, 1319−1331.

(24) Amirhosseini, H.; Najafi, F. Design, Prototyping and Performance Evaluation of a Bio-inspired Walking Microrobot. *Iran. J. Sci. Technol.* **2020**, *44*, 799−811.

(25) Zhang, J.; Song, G.; Li, Y.; Qiao, G.; Song, A.; Wang, A. A bio-inspired jumping robot: Modeling, simulation, design, and experimental results. *Mechatronics* **2013**, *23*, 1123−1140.

(26) Zhao, J.; Xu, J.; Gao, B.; Xi, N.; Cintrón, F. J.; Mutka, M. W.; Xiao, L. MSU Jumper: A Single-Motor-Actuated Miniature Steerable Jumping Robot. *IEEE Trans. Robot.* **2013**, *29*, 602−614.

(27) Singh, P.; Ananthasuresh, G. K. A Compact and Compliant External Pipe-Crawling Robot. *IEEE Trans. Robot.* **2013**, *29*, 251−260.

(28) Taylor, G. I. Analysis of the swimming of microscopic organisms. *Proc. R. Soc. London, Ser. A* **1951**, *209*, 447−461.

(29) Meissner, M. H.; Gloviczki, P.; Comerota, A. J.; Dalsing, M. C.; Eklof, B. G.; Gillespie, D. L.; Lohr, J. M.; McLafferty, R. B.; Murad, M. H.; Padberg, F.; Pappas, P.; Raffetto, J. D.; Wakefield, T. W. Early thrombus removal strategies for acute deep venous thrombosis: Clinical Practice Guidelines of the Society for Vascular Surgery and the American Venous Forum. *J. Vasc. Surg.* **2012**, *55*, 1449−1462.

(30) Yang, S.; Cao, C.; Sun, Y.; Huang, P.; Wei, F.; Song, W. Nanoscale Magnetic Stirring Bars for Heterogeneous Catalysis in Microscopic Systems. *Angew. Chem., Int. Ed.* **2015**, *54*, 2661−2664.

(31) Huang, H. W.; Uslu, F. E.; Katsamba, P.; Lauga, E.; Sakar, M. S.; Nelson, B. J. Adaptive locomotion of artificial microswimmers. *Sci. Adv.* **2019**, *5*, No. eaau1532.

(32) Liu, D.; Yang, Z.; Zhang, L.; Wei, M.; Lu, Y. Cell-free biology using remote-controlled digital microfluidics for individual droplet control. *RSC Adv.* **2020**, *10*, 26972−26981.

(33) Rasheed, M.; Wirth, T. Intelligent Microflow: Development of Self-Optimizing Reaction Systems. *Angew. Chem., Int. Ed.* **2011**, *50*, 357−358.

(34) Wan, L.; Song, H.; Chen, X.; Zhang, Y.; Yue, Q.; Pan, P.; Su, J.; Elzatahry, A. A.; Deng, Y. A Magnetic-Field Guided Interface Coassembly Approach to Magnetic Mesoporous Silica Nanochains for Osteoclast-Targeted Inhibition and Heterogeneous Nanocatalysis. *Adv. Mater.* **2018**, *30*, 1707515.

(35) Jørgensen, H.; Pinelo, M. Enzyme recycling in lignocellulosic biorefineries. *Biofuels, Bioprod. Biorefin.* **2017**, *11*, 150−167.

(36) Gao, S.; Lin, H.; Zhang, H.; Yao, H.; Chen, Y.; Shi, J. Nanocatalytic Tumor Therapy by Biomimetic Dual Inorganic Nanozyme-Catalyzed Cascade Reaction. *Adv. Sci.* **2019**, *6*, 1801733.

(37) Wu, X.; Ge, J.; Yang, C.; Hou, M.; Liu, Z. Facile synthesis of multiple enzyme-containing metal-organic frameworks in a biomolecule-friendly environment. *Chem. Commun.* **2015**, *51*, 13408−13411.

(38) Dawidowicz, A. L.; Olszowy, M. The importance of solvent type in estimating antioxidant properties of phenolic compounds by ABTS assay. *Eur. Food Res. Technol.* **2013**, *236*, 1099−1105.

(39) Liu, D.; Li, S.; Zhang, T.; Jiang, H.; Lu, Y. 3D Magnetic Field-Controlled Synthesis, Collective Motion, and Bioreaction Enhancement of Multifunctional Peasecod-like Nanochains. *ACS Appl. Mater. Interfaces* **2021**, *13*, 36157−36170.

(40) Wu, Z.; Li, L.; Yang, Y.; Hu, P.; Li, Y.; Yang, S.-Y.; Lihong, V. W.; Gao, W. A microrobotic system guided by photoacoustic computed tomography for targeted navigation in intestines in vivo. *Sci. Robot.* **2019**, *4*, No. eaax0613.

https://doi.org/10.1021/acsami.1c25102
ACS Appl. Mater. Interfaces XXXX, XXX, XXX−XXX